Comput Mech (2013) 52:463–483
DOI 10.1007/s00466-013-0823-1

ORIGINAL PAPER

Finite strain viscoelasticity: how to consistently couple discretizations in time and space on quadrature-point level for full order $p \geq 2$ and a considerable speed-up

Bernhard Eidel · Felipe Stumpf · Jörg Schröder

Received: 3 July 2012 / Accepted: 28 November 2012 / Published online: 12 February 2013
© Springer-Verlag Berlin Heidelberg 2013

Abstract In computational viscoelasticity, the spatial finite element discretization for the global solution of the weak form of the balance of momentum is *coupled* to the temporal discretization for solving local initial value problems (IVP) of viscoelastic flow. In this contribution we show that this global-local or space-time coupling is *consistent*, if the total strain tensor as the coupling quantity exhibits the same approximation order p in time as the Runge–Kutta (RK) integration algorithm. To this end we construct interpolation polynomials, based on data at t_{n+1}, t_n, ..., t_{n+2-p}, $p \geq 2$, which provide consistent strain data at RK stages. This is a generalization of the idea proposed in (Eidel and Kuhn, Int J Numer Methods Eng 87(11):1046–1073, 2011). For lower-order strain interpolation, time integration exhibits order reduction and therefore low efficiency. For consistent strain interpolation, the adapted RK methods up to $p = 4$ obtain full convergence order and thus approve the novel concept of consistency. High speed-up factors substantiate the improved efficiency compared with Backward-Euler.

Keywords Viscoelastic · Time integration · Space-time coupling · Finite element · Runge–Kutta methods

Dedicated to the memory of Juan Carlos Simó (1952-1994) on the occasion of his 60th birthday.

B. Eidel (✉) · J. Schröder
Institut für Mechanik, Fachbereich für Ingenieurwissenschaften/
Abtl. Bauwissenschaften, Universität Duisburg-Essen,
Universitätsstr. 15, 45117 Essen, Germany
e-mail: bernhard.eidel@uni-due.de

F. Stumpf
Universidade Federal do Rio Grande do Sul, Rau Sarmento Leite,
425-2°, Andar CEP: 90.050–170, Porto Alegre, RS, Brasil
e-mail: felipe.stumpf@ufrgs.br

1 Introduction

Time integration algorithms are the numerical workhorses in computational inelasticity, since they largely determine accuracy and efficiency. The very standard in time integration for inelastic constitutive laws is Backward–Euler (BE). It exhibits nice stability properties and along with its relative ease in implementation it is attractive, although it is only linear, [39].

Viscoelasticity models describe the material behavior of great many organic materials and biological substances like flesh, skin, bones and cells to name but a few, [41]. But also technical materials such as rubber, or polymers in general, exhibit viscoelastic characteristics, [2,3,6,33,35]. In younger scientific disciplines like e.g. in biomechanics, viscoelastic material models have already entered the patient-specific treatment via predictive finite element simulations. Here and in many other applications of viscoelastic finite element calculations, the simulations are time-critical and accuracy counts. For that aim, stable, fast and accurate time integration algorithms are of utmost importance.

Higher-order time integration methods are appealing, since they promise higher accuracy, and at best, higher efficiency than BE. That rises the following question.

1. *What is an advantageous algorithmic embedding of higher-order time integration methods $p \geq 2$ for viscoelasticity into nonlinear finite element frameworks? What has to be done, if the point of departure is BE?*

The choice of BE as the point of departure is adequate for at least two reasons. It is the very standard in inelastic finite element methods[1]. Moreover, diagonally implicit RK

[1] That applies to BE as the integrator for inelastic rate equations, but not for integrating the equations of structural dynamics.

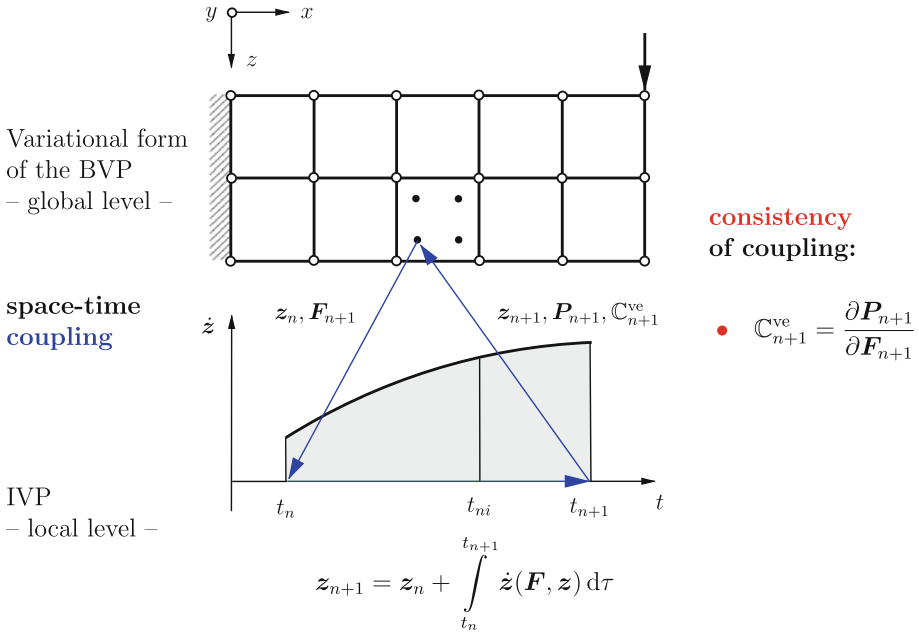

Fig. 1 Scheme for the coupling of spatio-temporal discretizations in viscoelastic finite element simulations for BE. In this representation, $\boldsymbol{F}$ is the deformation gradient, $\boldsymbol{z}$ denotes the set of internal variables, $\boldsymbol{P}$ is the First Piola–Kirchhoff stress tensor, $\mathbb{C}^{ve}_{n+1}$ denotes the algorithmically consistent tangent.

(DIRK) methods, which are used in the present work, have the same algorithmic structure as BE making the upgrade to higher-order DIRK methods feasible with ease.

The answer to the first question shall be given from a fresh, new look onto the standard algorithmic structure of finite element frameworks for the solution of inelastic problems, cf. [8]. Following this structure, the space-discrete, variational form of the balance of momentum leads to a set of nonlinear algebraic equations, which are solved on the *global level* for the primary unknowns, typically displacements (in mixed methods stresses as well). Total strains as derived from displacements are passed over to and serve as input for the solution of the initial value problems (IVP) of inelastic flow on quadrature-point (typically Gauss-point) level, which is termed the *local level* in this context. This kind of global-local or space-time *coupling* with a total deformation measure (here: the deformation gradient $\boldsymbol{F}$) as the coupling quantity is schematically displayed in Fig. 1. Time integration of the viscoelastic evolution equations yield an update of viscoelastic strains (here: $\boldsymbol{z}$) and the total stresses (here: $\boldsymbol{P}$). Since Newton's method is typically used for the solution of the set of nonlinear algebraic equations on the global level, linearizations are necessary for the sake of quadratic convergence. Within this solution framework employing linearizations, the classical meaning of *consistency* is that the tangent is consistent with the chosen time integration method, therefore called *algorithmically consistent tangent moduli*, which goes back to [36,40]. The tangent $\mathbb{C}^{ve}_{n+1}$ and the updated stresses $\boldsymbol{P}_{n+1}$ are passed over to new iterations of the variational form of the balance of momentum until equilibrium is fulfilled, see Fig. 1 and its caption.

Two algorithmic variants can be distinguished. The first one, termed the *partitioned* ansatz, is the classical approach in computational inelasticity. It solves for equilibrium only at t_n, t_{n+1}, but not in the interior of the time interval at the stages of a multi-stage method like the midpoint-rule, or generally, any RK method.

Ellsiepen and Hartmann [12,20] have opened a door to higher-order methods in inelasticity by their proposal of a different concept, termed DAE/MLNA, for Differential Algebraic Equations along with a Multi-Level Newton Algorithm. This novel approach solves for global equilibrium additionally at the RK stages of the time interval. Although this procedure increases the computational costs compared with the traditional partitioned ansatz, the benefits of the achieved high order are predominant in that they lead to a considerably improved speed-up compared with BE, see the work of Hartmann for viscoelasticity, [20]. This approach is theoretically sound and a viable solution and thus answers the above first question.

Notwithstanding, the question naturally arises, whether the partitioned ansatz as described above and schematically displayed for BE in Fig. 1 can also be used along with higher-order RK methods. If so, a combination of the benefits from higher order *and* the lower complexity compared with the DAE/MLNA-approach could be realized. As it will turn out in the paper, the sketch for BE in Fig. 1 is not *complete* to realize this goal.

Instead, a novel, nonstandard aspect comes into play, which, if neglected for $p \geq 2$, leads to low accuracy, to a reduced convergence order compared with the nominal order (so-called *order reduction*), and, as a consequence,

to an inferior efficiency. It will be shown in Sect. 5, that these severe drawbacks can lead to an overall performance of higher-order RK methods, which can be even worse than BE.

To obtain full convergence order in the partitioned ansatz, a completion of the scheme in Fig. 1 with respect to the *consistency* in coupling is necessary. The addressed consistency is intimately related to the characteristic of inelasticity, that RK methods, which are one-step, multi-stage schemes, require the calculation of total strains at the RK-stages. These RK stages are indicated in Fig. 1 by the mark for t_{ni} on the time axis. This leads to the next main question:

2. *In which format shall the total strain tensor be plugged into the RK stages for higher-order $p \geq 2$? Is a constant total strain in the time step sufficient, like for BE? If not, why not - and what else is correct?*

In [9] it is analyzed that the order of time integration crucially relies on the approximation order of total strain in time. More precisely, RK methods of order 3 require total strains of the approximation order 3. Complementary, linear interpolation of strain, based on t_n and t_{n+1} data, thus introducing an approximation error of order 2, leads to an order reduction of time integration to order 2.

The objective of the present contribution is a generalization of the ideas in [9] with the aim to achieve full convergence order in time integration for viscoelastic constitutive models at finite strains. This doing we focus on DIRK methods up to order 4. DIRK methods are particularly efficient RK methods with nice stability properties also for stiff problems.

The ultimate question to be answered in the present work is this.

3. *Do higher-order RK-methods significantly improve the efficiency in viscoelastic finite element simulations?*

If the full convergence order is obtained, RK methods which exhibit A- and S-stability allow for much larger time step sizes than BE, the stable but sedate standard for inelastic time integration. While RK methods are well known for their higher accuracy based on higher convergence order, a recommendation to use them must be based on a significant speed-up in simulations compared with BE.

The structure of the present paper follows the main objectives:

(i) Presentation of the algorithmic structure of finite element methods for the solution of inelastic initial boundary value problems (IBVP). Here, the focus is on the coupling of the global BVP with the local IVPs via total strains as coupling agencies. The aspect of *consistency* of coupling is crucial for the way of constructing total strains at the stages of higher-order RK methods. The generalization of the introductory picture in Fig. 1 is the content of Sect. 4 and will answer the above questions 1.) and 2.).

(ii) Description of the algorithmic treatment of a finite-strain viscoelasticity model as outlined in Sect. 2.2 using DIRK methods up to order 4, see the Appendix Section, along with our novel concept of consistent strain interpolation.

(iii) Numerical assessment of the presented methodology to check accuracy, convergence order and efficiency. This is carried out in Sect. 5 and the results answer the above third question.

2 Constitutive framework

We consider a body $\Omega \subset \mathbb{R}^3$ undergoing a viscoelastic deformation $\varphi : \Omega \to \mathbb{R}^3$ with the deformation gradient $\boldsymbol{F} = \partial_{\boldsymbol{X}} \varphi(\boldsymbol{X})$ and the Jacobian $J = \det \boldsymbol{F} > 0$, where $\boldsymbol{X}$ is a material point in the reference configuration.

2.1 Decompositions of deformation

The deformation gradient $\boldsymbol{F}$ can be decomposed into

$$\boldsymbol{F} = \hat{\boldsymbol{F}}\, \bar{\boldsymbol{F}} \tag{1}$$

with the volumetric part $\hat{\boldsymbol{F}}$ and the isochoric part $\bar{\boldsymbol{F}}$ defined as

$$\hat{\boldsymbol{F}} = J^{1/3}\, \boldsymbol{1}, \qquad \det \hat{\boldsymbol{F}} = \det \boldsymbol{F} = J\,, \tag{2}$$

$$\bar{\boldsymbol{F}} = J^{-1/3}\, \boldsymbol{F}, \qquad \det \bar{\boldsymbol{F}} = 1. \tag{3}$$

Various material models are based on the decomposition (1), since it allows to introduce stress tensors, which exhibit the same decomposition as the deformations.

From (1), the unimodular Right-Cauchy-Green tensor is motivated as

$$\bar{\boldsymbol{C}} = \bar{\boldsymbol{F}}^T\, \bar{\boldsymbol{F}} = \bar{\boldsymbol{U}}^2 = J^{-2/3} \boldsymbol{C}\,, \qquad \det \bar{\boldsymbol{C}} = 1. \tag{4}$$

The main invariants of $\bar{\boldsymbol{C}}$ are

$$I_{\bar{C}} = \operatorname{tr} \bar{\boldsymbol{C}}\,, \quad II_{\bar{C}} = \frac{1}{2}\left((\operatorname{tr} \bar{\boldsymbol{C}})^2 - \operatorname{tr} \bar{\boldsymbol{C}}^2 \right)\,,$$
$$III_{\bar{C}} = \det \bar{\boldsymbol{C}} = 1. \tag{5}$$

The multiplicative decomposition of the deformation gradient

$$\boldsymbol{F} = \boldsymbol{F}^e\, \boldsymbol{F}^{\mathrm{v}} \tag{6}$$

into the elastic part $\boldsymbol{F}^{\mathrm{e}}$ and the inelastic part $\boldsymbol{F}^{\mathrm{v}}$ was originally introduced for metal plasticity, cf. Kröner and Lee [28,30]. This decomposition has been equally used for the modeling of viscoelasticity at finite strains for a variety of non-metallic materials, [3,2,6,7,14,20,26,27,33,35,38].

Table 1 Constitutive model of finite strain viscoelasticity

Split of deformation	$\boldsymbol{F} = \boldsymbol{F}^{\mathrm{e}}\,\boldsymbol{F}^{\mathrm{v}}, \quad \boldsymbol{C} = \boldsymbol{F}^{T}\boldsymbol{F}, \quad \bar{\boldsymbol{C}} = J^{-1/3}\boldsymbol{F}$	(7)
Decomposition of stress	$\boldsymbol{S} = \boldsymbol{S}^{\mathrm{eq}}_{\mathrm{vol}} + \boldsymbol{S}^{\mathrm{eq}}_{\mathrm{iso}} + \boldsymbol{S}^{\mathrm{ov}}$	(8)
Equilibrium stress	$\boldsymbol{S}^{\mathrm{eq}}_{\mathrm{vol}} = JU'(J)\boldsymbol{C}^{-1}$, with $U'(J) = \frac{K}{10}(J^4 - J^{-6})$	(9)
	$\boldsymbol{S}^{\mathrm{eq}}_{\mathrm{iso}} = \varphi_1\,\mathbf{1} + \varphi_2\,\bar{\boldsymbol{C}} + \varphi_3\,\bar{\boldsymbol{C}}^{-1}$	(10)
	$\varphi_1 = 2(\det \boldsymbol{C})^{-1/3}(w_1 + w_2\, I_{\bar{C}})$	(11)
	$\varphi_2 = -2(\det \boldsymbol{C})^{-1/3} w_2$	(12)
	$\varphi_3 = -\frac{2}{3}(\det \boldsymbol{C})^{-1/3}(w_1 I_{\bar{C}} + 2w_2 II_{\bar{C}})$	(13)
	$w_1 = \frac{\partial w^{\mathrm{eq}}}{\partial I_{\bar{C}}} = c_{10} + 3c_{30}(I_{\bar{C}} - 3)^2$	(14)
	$w_2 = \frac{\partial w^{\mathrm{eq}}}{\partial II_{\bar{C}}} = c_{01}$	(15)
Overstress	$\boldsymbol{S}^{\mathrm{ov}} = 2\mu\,\frac{(\det \boldsymbol{C}^{\mathrm{v}})^{1/3}}{(\det \boldsymbol{C})^{1/3}}\left(\boldsymbol{C}^{\mathrm{v}-1} - \frac{1}{3}(\boldsymbol{C} : \boldsymbol{C}^{\mathrm{v}-1})\boldsymbol{C}^{-1}\right)$	(16)
Flow rule	$\dot{\boldsymbol{C}}^{\mathrm{v}} = \frac{4\mu}{\eta}\,\frac{(\det \boldsymbol{C}^{\mathrm{v}})^{1/3}}{(\det \boldsymbol{C})^{1/3}}\left(\boldsymbol{C} - \frac{1}{3}(\boldsymbol{C} : \boldsymbol{C}^{\mathrm{v}-1})\boldsymbol{C}^{\mathrm{v}}\right)$	(17)

2.2 A viscoelasticity model at finite strains

In the following, the finite strain viscoelasticity model as proposed in [20] is briefly described. In the context of the present paper, the model serves the purpose to prove, that our novel algorithmic contributions can empower RK schemes to achieve full convergence order up to $p = 4$ in time integration of viscoelastic flow. For a comprehensive analysis of continuum viscoelasticity models we refer to the monographs [25,29]. Algorithmic aspects for the treatment of viscoelasticity in the finite element method can be found in e.g. [31], [22] and with a particular focus on structural dynamics in [15].

The assumptions for the material model to be introduced are the following, [20]. The material is isotropic and exhibits quasi-incompressible behavior. Hydrostatic stresses exclusively arise from elasticity. The deformations extend into the regime of finite strains, which requires a geometrically nonlinear theory. The material exhibits velocity-dependent, nonlinear phenomena. A hysteresis of equilibrium stress states is negligible, such that viscoelasticity is adequate. The equilibrium stresses are derived from a hyperelasticity relation. All processes considered are isothermal. For extensions to non-isothermal processes, see e.g. [32] or [38]; for the consideration of the Payne effect, see [33].

The model is summarized in Table 1. The total stress tensor $\boldsymbol{S}$ in (8) is the 2nd Piola–Kirchhoff stress tensor, which can be additively decomposed into an equilibrium part $\boldsymbol{S}^{\mathrm{eq}}$ and an overstress part $\boldsymbol{S}^{\mathrm{ov}}$. According to (9), $\boldsymbol{S}^{\mathrm{eq}}_{\mathrm{vol}}$ is the volumetric part of the equilibrium stress tensor; its isochoric part is defined according to (10) in terms of $\mathbf{1}$, $\bar{\boldsymbol{C}}$, $\bar{\boldsymbol{C}}^{-1}$ and in terms of the scalar functions $\varphi_1, \varphi_2, \varphi_3$ according to (11)–(13). Therein, the variables w_1 and w_2 are defined as derivatives of w^{eq} with respect to the invariants $I_{\bar{C}}$ and $II_{\bar{C}}$, respectively. The evolution equation for the viscoelastic strain $\boldsymbol{C}^{\mathrm{v}}$ is given in (17), for the overstress $\boldsymbol{S}^{\mathrm{ov}}$ in (16).

The isotropic viscoelasticity model exhibits the following set of material parameters; the compression modulus K, the shear modulus μ, the elastic constants c_{10}, c_{30}, c_{01} and the viscosity η.

The above viscoelastic model falls into the general class of constitutive equations of the type

$$\boldsymbol{S} = \boldsymbol{h}(\boldsymbol{C}, \boldsymbol{z}) \tag{18}$$

$$\dot{\boldsymbol{z}} = \boldsymbol{f}(\boldsymbol{C}, \boldsymbol{z})\,, \qquad \boldsymbol{z}(t_0) = \boldsymbol{z}_0\,, \tag{19}$$

where (18) denotes an elasticity relation and $\boldsymbol{z} \in \mathbb{R}^{n_z}$ defines a set of internal variables describing viscoelastic material behavior. Here, $\boldsymbol{z} = \{\boldsymbol{C}^{\mathrm{v}}\}$ with $n_z = 6$ for the 3D case of symmetric strain measures.

3 Time Integration

To put things into perspective, we briefly recall in the Appendix basic equations for the numerical solution of an IVP by implicit RK (IRK) methods, cf. e.g. [17–19]. Moreover, the characteristics and benefits of the class of Diagonally Implicit RK (DIRK) methods are reiterated to keep the paper self-contained.

3.1 Application of DIRK schemes to finite strain viscoelasticity

In the following, DIRK schemes are applied to the evolution equations of viscoelasticity. Note, that the choice for DIRK schemes as a particular class of RK schemes as well as the

choice for the viscoelasticity model is without loss of generality for our framework.

The evolution equation for the viscoelastic Right Cauchy-Green strain tensor reads as

$$\dot{\boldsymbol{C}}^{\mathrm{v}} = \frac{4\mu}{\eta}\frac{(\det \boldsymbol{C}^{\mathrm{v}})^{1/3}}{(\det \boldsymbol{C})^{1/3}}\left(\boldsymbol{C} - \frac{1}{3}(\boldsymbol{C} : \boldsymbol{C}^{\mathrm{v}-1})\boldsymbol{C}^{\mathrm{v}}\right). \tag{20}$$

After discretization in time, the application of a DIRK method yields the update formula for $\boldsymbol{C}^{\mathrm{v}}_{ni}$ at stage i in the time interval $\Delta t_n = [t_n, t_{n+1}]$

$$\boldsymbol{C}^{\mathrm{v}}_{ni} = \boldsymbol{\Sigma}^{\mathrm{v}}_{ni} + \Delta t_n a_{ii}\dot{\boldsymbol{C}}^{\mathrm{v}}_{ni}\,, \tag{21}$$

$$\text{with} \qquad \boldsymbol{\Sigma}^{\mathrm{v}}_{ni} = \boldsymbol{C}^{\mathrm{v}}_{n} + \Delta t_n \sum_{j=1}^{i-1} a_{ij}\dot{\boldsymbol{C}}^{\mathrm{v}}_{nj}\,, \tag{22}$$

where $\boldsymbol{C}^{\mathrm{v}}_{n} \approx \boldsymbol{C}^{\mathrm{v}}(t_n)$. With (20) a reformulation of (21) yields

$$\frac{\boldsymbol{C}^{\mathrm{v}}_{ni} - \boldsymbol{\Sigma}^{\mathrm{v}}_{ni}}{\Delta t_n a_{ii}} - \frac{4\mu}{\eta}\frac{(\det \boldsymbol{C}^{\mathrm{v}}_{ni})^{1/3}}{(\det \boldsymbol{C}(t_{ni}))^{1/3}} \times \left(\boldsymbol{C}(t_{ni}) - \frac{1}{3}(\boldsymbol{C}(t_{ni}) : \boldsymbol{C}(t_{ni})^{\mathrm{v}-1})\boldsymbol{C}^{\mathrm{v}}_{ni}\right) = \boldsymbol{0}. \tag{23}$$

In order to reduce the numerical effort for the solution of 6 nonlinear algebraic equations for $\boldsymbol{C}^{\mathrm{v}}_{ni}$, the following reformulation as proposed in the work of [22] is instrumental

$$\boldsymbol{C}^{\mathrm{v}}_{ni} = \frac{1}{g(\boldsymbol{C}^{\mathrm{v}}_{ni})}\,\boldsymbol{\xi}(\boldsymbol{C}^{\mathrm{v}}_{ni}) \tag{24}$$

with the scalar function $g(\boldsymbol{C}^{\mathrm{v}}_{ni})$ and the tensorial function $\boldsymbol{\xi}(\boldsymbol{C}^{\mathrm{v}}_{ni})$ according to

$$g(\boldsymbol{C}^{\mathrm{v}}_{ni}) = 1 + \frac{4}{3}\frac{\Delta t_n a_{ii}\mu}{\eta}\frac{(\det \boldsymbol{C}^{\mathrm{v}}_{ni})^{1/3}}{(\det \boldsymbol{C}(t_{ni}))^{1/3}}(\boldsymbol{C}(t_{ni}) : \boldsymbol{C}^{\mathrm{v}-1}_{ni})\,, \tag{25}$$

$$\boldsymbol{\xi}(\boldsymbol{C}^{\mathrm{v}}_{ni}) = \boldsymbol{\Sigma}^{\mathrm{v}}_{ni} + \frac{4\Delta t_n a_{ii}\mu}{\eta}\frac{(\det \boldsymbol{C}^{\mathrm{v}})^{1/3}}{(\det \boldsymbol{C}(t_{ni}))^{1/3}}\boldsymbol{C}(t_{ni}). \tag{26}$$

Two scalars can be identified in the update formula

$$x_1 := (\det \boldsymbol{C}^{\mathrm{v}}_{ni})^{1/3} \tag{27}$$

$$x_2 := \boldsymbol{C}(t_{ni}) : \boldsymbol{C}^{\mathrm{v}-1}_{ni} \tag{28}$$

which are used as unknowns in the following replacing the 6 components of $\boldsymbol{C}^{\mathrm{v}}$

$$\Phi_m(x_1, x_2) = 0 \qquad m = 1, 2 \tag{29}$$

with

$$\Phi_1(x_1, x_2) := x_1 - g^{-1}(\det \boldsymbol{\xi})^{1/3}\,, \tag{30}$$

$$\Phi_2(x_1, x_2) := x_2 - g\,\boldsymbol{\xi}^{-1} : \boldsymbol{C}_{ni}\,, \tag{31}$$

where we use the abbreviations

$$g = g(x_1, x_2) = 1 + \frac{\hat{k}}{3}\frac{x_1 x_2}{\eta}\,, \tag{32}$$

$$\boldsymbol{\xi} = \boldsymbol{\xi}(x_1, x_2) = \boldsymbol{\Sigma}^{\mathrm{v}}_{ni} + \hat{k}\frac{x_1}{\eta}\boldsymbol{C}_{ni}\,, \tag{33}$$

$$\text{and} \quad \hat{k} = \frac{4\mu\Delta t_n a_{ii}}{(\det \boldsymbol{C}_{ni})^{1/3}}. \tag{34}$$

The application of Newton's method for the solution of this set of nonlinear equations yields for each iteration step (r) the following set of linear equations

$$\begin{bmatrix} \Phi_{1,1} & \Phi_{1,2} \\ \Phi_{1,2} & \Phi_{2,2} \end{bmatrix}^{(r)} \begin{bmatrix} \Delta x_1 \\ \Delta x_2 \end{bmatrix} = -\begin{bmatrix} \Phi_1 \\ \Phi_2 \end{bmatrix}^{(r)} \tag{35}$$

with increments $\Delta x_m = x_m^{(r+1)} - x_m^{(r)}$.

For the last stage $i = s$, which coincides with the end of the time interval t_{n+1}, the solution x_1, x_2 is used for the computation of the viscoelastic overstress

$$\boldsymbol{S}^{\mathrm{ov}}_{n+1} = \frac{2\mu\, x_1}{(\det \boldsymbol{C}_{ni})^{1/3}}\left(g(x_1, x_2)\,\boldsymbol{\xi}^{-1}(x_1, x_2) - \frac{1}{3}x_2\,\boldsymbol{C}^{-1}_{ns}\right). \tag{36}$$

Remarks

1. The coefficients of the DIRK-matrix $A = [a_{ij}]_{i,j=1,\ldots,s}$ in (21) and (22) are chosen from Table 17 in the Appendix. The weighting factors b_i remain hidden for stiffly accurate DIRK methods due to $a_{si} = b_i$, and the coefficients c_i from Table 17 in the Appendix enter $\boldsymbol{C}^{\mathrm{v}}_{ni}$ via $t_{ni} = t_n + c_i\Delta t_n$.
   There is no ambiguity nor free choice for the quantities in time integration except of for the stage values $\boldsymbol{C}(t_{ni})$. How to approximate them $\boldsymbol{C}_{ni} \approx \boldsymbol{C}(t_{ni})$ in a *consistent* manner is the key question and will be answered in the following Sect. 4.
2. Note that the update of DIRK methods for each decoupled stage solution according to (21) and (22) covers BE as a special case (BE is a DIRK method with $p = 1$). This fact underlines the relative ease of implementing higher order DIRK methods for a viscoelastic constitutive law, if BE is already implemented.

4 Space-time coupling

4.1 General idea

According to the finite element solution of inelasticity the variational form of the balance of momentum is solved on

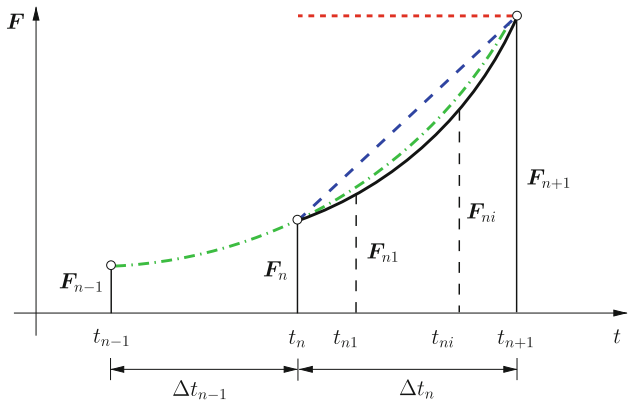

Fig. 2 The exact, unknown deformation path in time (black, full line) and its approximations via constant deformation $\boldsymbol{F} = \boldsymbol{F}_{n+1}$ (red, dotted line) and via linear (blue, dashed line), and quadratic (green, dashed-dotted line) interpolation

the global level for displacements as primary unknowns. Displacements as kinematical quantities are required as input for the solution of the IVP of inelastic flow on the local quadrature point (typically Gauss-point) level in each finite element. Since RK methods are one-step, multiple-stage schemes, their use in time integration requires the calculation of the total strain values at the RK-stages, see (23) and remark 1 in Sect. 3.1.

The most simple way to provide total strains at RK stages is to use throughout constant strain values in the time interval, say values at t_{n+1}. This is the way how it is done for BE, cf. $\boldsymbol{F}(t) = \boldsymbol{F}_{n+1} = \text{const.}$ for $t \in [t_n, t_{n+1}]$, cf. Fig. 1.

Figure 2 illustrates, that the exact strain path in time is typically nonlinear for viscoelastic problems. Obviously, the approximation of deformation by a constant value is very inaccurate. The strain path can be better approximated by means of quadratic interpolation compared with linear interpolation.

In [9] it was analyzed that the approximation order of total strains in time rules the consistency order of viscoelastic time integration. More precisely it was shown, that a linear representation of strains based on t_n and t_{n+1} data introduces an approximation error of order 2 and therefore bounds the order of convergence in time integration to order 2. Similarly, quadratic strain interpolation to approximate the values at the RK stages introduces an approximation error of $\mathcal{O}(\Delta t^3)$ and enables a corresponding consistency and convergence order of 3 in time integration. Furthermore, it is shown in [9] that the construction of a third-order polynomial can be effectively based on time data t_n, t_{n+1} and additionally t_{n-1} as shown in Fig. 2. Of course, the accuracy of strain approximation in time by higher-order polynomials crucially relies on the *smoothness* of the strain path in time. For elasto-plasticity quite in contrast to viscoelasticity, the smoothness of strain paths depends on material parameters, which was analyzed for the first time in [10].

4.2 Consistency

The choice of the correct interpolation polynomial follows from a consistency analysis, which was proposed in [8]. The ODE

$$\dot{\boldsymbol{z}} = \boldsymbol{f}\left(\boldsymbol{F}(t), \boldsymbol{z}(t)\right) \tag{37}$$

describing viscoelastic flow is solved by a time integration algorithm of the nominal order p. Since the time-dependent deformation gradient $\boldsymbol{F}(t)$ serves as argument in (37), its approximation order in time does influence the order of time integration. This dependency is obvious but has been neglected in previous works with the exception of [9].

An interpolation polynomial of degree $q-1$ for the total strain introduces a corresponding approximation error of the order

$$\boldsymbol{F} = \mathcal{O}(\Delta t^q) \tag{38}$$

which implies that due to (37) q is an upper bound for the convergence order in time integration. More generally, it holds, cf. [8]

$$\boldsymbol{z} = \mathcal{O}(\Delta t^{\min\{p,q\}}). \tag{39}$$

Two conclusions are obvious. First, to empower time integration to its full order, the order of strain approximation and the order of time integration must be consistent, $q = p$. Second, a polynomial of lower order $q = p - m$, $m \geq 1$ will reduce the consistency order of the differential variable $\boldsymbol{z}$ and, as a consequence, of the stress tensor $\boldsymbol{P}$ as well.

Hence, the concept of consistency of space-time (or global-local) coupling in viscoelasticity, which was displayed in Fig. 1 in the introduction section, must be augmented according to Fig. 3; the novel condition $q = p$ ensures, that the nominal consistency order[2] in time integration can be obtained, while the standard condition of the algorithmically consistent tangent moduli $\mathbb{C}^{\text{ve}}_{n+1} = \partial \boldsymbol{P}_{n+1}/\partial \boldsymbol{F}_{n+1}$ ensures quadratic convergence in the solution of the linearized algebraic equations following from FEM-discretization of the weak form. The latter concept was introduced into computational inelasticity by Nagtegaal in [36] and generalized by Simó and Taylor in [40].

[2] To obtain the same *convergence* order as the *consistency* order, the stability of the time integrator has to be shown. Here we postpone the consideration of the convergence order to explicit numerical tests in Sect. 5.

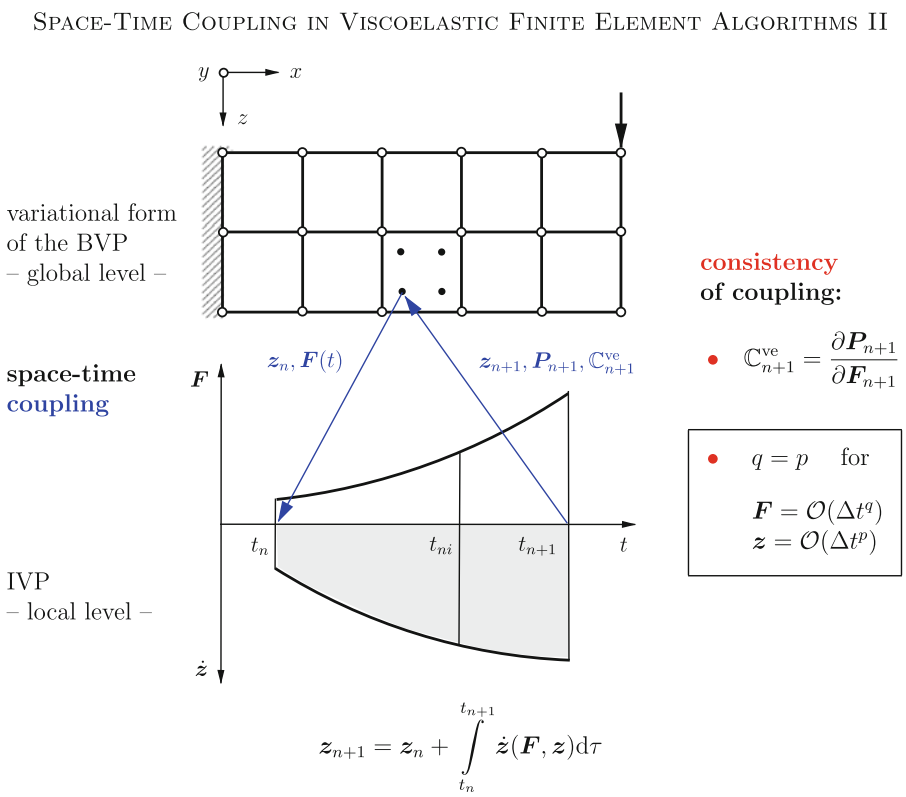

Fig. 3 Augmented scheme for the consistent coupling of spatio-temporal discretizations in viscoelastic finite element simulations for higher order methods $p \geq 2$ according to [8]. In this representation, $\boldsymbol{F}$ is the deformation gradient, $\boldsymbol{z}$ denotes the set of internal variables, $\boldsymbol{P}$ is the First Piola–Kirchhoff stress tensor, $\mathbb{C}^{ve}_{n+1}$ denotes the algorithmic tangent, which is consistent to the time integrator.

4.3 Constructing interpolation polynomials for consistent coupling

Returning to the viscoelastic model of the present work, we adapt the above considerations to the present setting. Hence, the set $\{\boldsymbol{z}, \boldsymbol{F}, \boldsymbol{P}\}$ is replaced by the quantities $\{\boldsymbol{C}^v, \boldsymbol{C}, \boldsymbol{S}\}$. In the following, the above consistency requirement for total strain approximation is fulfilled by interpolation polynomials of degree $q-1$ with $q = p$.

4.3.1 The case $p = 1$: stage values for constant total strain

The simplest way to determine the stage values at time $t = t_{ni} = t_n + c_i \Delta t$ is via a constant approximation of the total strain tensor $\boldsymbol{C}(t) = \boldsymbol{C}_{n+1}$. Introducing a new time scale $\tilde{t} := t - t_n$ in the time interval $t \in [t_n, t_{n+1}]$ and a corresponding polynomial $\boldsymbol{p}_0(t)$ yields the approximation of $\boldsymbol{C}(t)$

$$\boldsymbol{C}(t = t_{ni}) \approx \boldsymbol{p}_0(\tilde{t} = c_i \Delta t) = \boldsymbol{C}_{n+1}. \tag{40}$$

Under the assumption that the strains in the time interval $t \in [t_n, t_{n+1}]$ and $\tilde{t} \in [0, \Delta t]$ are continuously differentiable, the interpolation error in the strains is $|\boldsymbol{C}(\tilde{t}) - \boldsymbol{p}_0(\tilde{t})| \leq M_1(\Delta t)$ with $M_1 = \max\{|\boldsymbol{C}'(\tilde{t})| : \tilde{t} \in [0, \Delta t]\}$.

Remark BE fulfils the condition $q = p$, since the constant strain approximation $\boldsymbol{F} = \boldsymbol{F}_{n+1}$ implying $q = 1$ is consistent with the linear order, $p = 1$.

4.3.2 The case $p = 2$: stage values via linear interpolation

With the new time scale $\tilde{t} := t - t_n$, the linear interpolation polynomial, supported by $(0, \boldsymbol{C}_n)$ and $(\Delta t, \boldsymbol{C}_{n+1})$, reads $\boldsymbol{p}_1(\tilde{t}) = \boldsymbol{C}_n + \tilde{t}/\Delta t(\boldsymbol{C}_{n+1} - \boldsymbol{C}_n)$, which leads to the approximation of $\boldsymbol{C}(t)$ at time $t = t_{ni} = t_n + c_i \Delta t$

$$\boldsymbol{C}(t = t_{ni}) \approx \boldsymbol{p}_1(\tilde{t} = c_i \Delta t) = \boldsymbol{C}_n + c_i(\boldsymbol{C}_{n+1} - \boldsymbol{C}_n). \tag{41}$$

Under the assumption that total strains in the time interval $t \in [t_n, t_{n+1}]$ and $\tilde{t} \in [0, \Delta t]$ are twice continuously differentiable, the interpolation error in the strains is $|\boldsymbol{C}(\tilde{t}) - \boldsymbol{p}_1(\tilde{t})| \leq M_2/2(\Delta t)^2$ with $M_2 = \max\{|\boldsymbol{C}''(\tilde{t})| : \tilde{t} \in [0, \Delta t]\}$.

Remark The calculation of stage values via linear interpolation was applied in [4] for elasto-plasticity. In this work however, an order reduction of a fully implicit, 3rd order RK method to order 2 was observed, which is in agreement to the consistency to the consistency considerations in Sect. 4.2.

4.3.3 The case $p = 3$: stage values via quadratic interpolation

The fact that the error for linear interpolation is of the order $\mathcal{O}(\Delta t^2)$ suggests that this low-order approximation is a candidate to cause order reduction in viscoelastic stress computation when higher-order methods, $p \geq 3$ are used. Based on this hypothesis we propose a quadratic

interpolation polynomial $\boldsymbol{p}_2(\tilde{t})$, which is based on the data set $(-\Delta t, \boldsymbol{C}_{n-1})$, $(0, \boldsymbol{C}_n)$ and $(\Delta t, \boldsymbol{C}_{n+1})$. Given that $\boldsymbol{C}(\tilde{t})$ is three times continuously differentiable in $[-\Delta t, \Delta t]$, it holds for the interpolation error $|\boldsymbol{C}(\tilde{t}) - \boldsymbol{p}_2(\tilde{t})| \leq M_3/6(\Delta t^3)$ with $M_3 = \max\{|\boldsymbol{C}'''(\tilde{t})| : \tilde{t} \in [-\Delta t, \Delta t]\}$.

The interpolation polynomial $\boldsymbol{p}_2$ reads

$$\boldsymbol{p}_2(\tilde{t}) = \frac{1}{2\Delta t^2}(\boldsymbol{C}_{n-1} - 2\boldsymbol{C}_n + \boldsymbol{C}_{n+1})\,\tilde{t}^2 + \frac{1}{2\Delta t}(\boldsymbol{C}_{n+1} - \boldsymbol{C}_{n-1})\,\tilde{t} + \boldsymbol{C}_n. \tag{42}$$

With (42) it follows for the stage values of $\boldsymbol{C}$ at $t = t_{ni} = t_n + c_i\Delta t$ and $\tilde{t} = c_i\Delta t$

$$\boldsymbol{C}(t = t_{ni}) \approx \boldsymbol{p}_2(\tilde{t} = c_i\Delta t) = \frac{c_i}{2}(c_i - 1)\,\boldsymbol{C}_{n-1} + (1 - c_i^2)\,\boldsymbol{C}_n + \frac{c_i}{2}(c_i + 1)\,\boldsymbol{C}_{n+1}. \tag{43}$$

4.3.4 The case $p = 4$: stage values via cubic interpolation

For convergence order 4 in time integration, the consistent interpolation polynomial for total strain is of degree 3. Hence, 4 data points are necessary. They are chosen to be $(-\Delta t_{n-2}, \boldsymbol{C}_{n-2})$, $(-t_{n-1}, \boldsymbol{C}_{n-1})$, $(0, \boldsymbol{C}_n)$, $(\Delta t_n, \boldsymbol{C}_{n+1})$. Given that $\boldsymbol{C}(\tilde{t})$ is four times continuously differentiable in $[-2\Delta t, \Delta t]$, it holds for the interpolation error $|\boldsymbol{C}(\tilde{t}) - \boldsymbol{p}_3(\tilde{t})| \leq M_4/24(\Delta t^4)$, with $M_4 = \max\{|\boldsymbol{C}''''(\tilde{t})| : \tilde{t} \in [-2\Delta t, \Delta t]\}$.

$$\boldsymbol{p}_3(t) = \sum_{i=0}^{3} \boldsymbol{f}(t_{ni})\boldsymbol{l}_i(t_{ni}) \tag{44}$$

where

$$\boldsymbol{l}_0 = \frac{(t_{ni} - t_{n-1})(t_{ni} - t_n)(t_{ni} - t_{n+1})}{(t_{n-2} - t_{n-1})(t_{n-2} - t_n)(t_{n-2} - t_{n+1})}\,\boldsymbol{C}_{n-2} \tag{45}$$

$$\boldsymbol{l}_1 = \frac{(t_{ni} - t_{n-2})(t_{ni} - t_n)(t_{ni} - t_{n+1})}{(t_{n-1} - t_{n-2})(t_{n-1} - t_n)(t_{n-1} - t_{n+1})}\,\boldsymbol{C}_{n-1} \tag{46}$$

$$\boldsymbol{l}_2 = \frac{(t_{ni} - t_{n-2})(t_{ni} - t_{n-1})(t_{ni} - t_{n+1})}{(t_n - t_{n-2})(t_n - t_{n-1})(t_n - t_{n+1})}\,\boldsymbol{C}_n \tag{47}$$

$$\boldsymbol{l}_3 = \frac{(t_{ni} - t_{n-2})(t_{ni} - t_{n-1})(t_{ni} - t_n)}{(t_{n+1} - t_{n-2})(t_{n+1} - t_{n-1})(t_{n+1} - t_n)}\,\boldsymbol{C}_{n+1}. \tag{48}$$

Remark Note that for $p \geq 3$ a change in the step size affects the total strain interpolation due to its multi-step characteristic. General aspects of mathematical interpolation have to be considered like the distance between the nodes of interpolation in order to avoid artifacts like oscillatoric effects. In the present analysis we keep the time step size fixed, since only in that case the uniform convergence order shows up.

Table 2 displays the time integration algorithm using DIRK schemes of order p =2-4 along with the novel concept of consistent strain interpolation.

4.4 Conceptual comparison with DAE/MLNA

The perspective onto the IBVP of inelasticity as a global set of differential algebraic equations (DAE) and its solution by higher-order RK methods was introduced for rate-independent elasto-plasticity in [12], for viscoelasticity in [20,21] and applied to viscoelastic high-porosity foams in [34]. The solution method is termed DAE/MLNA for Differential Algebraic Equation/Multi-Level Newton Approach. It was shown that this method can achieve full convergence order up to order 3 and that it can considerably improve the efficiency compared with BE. The gain in efficiency of DAE/MLNA was observed, although it requires a solution of the global algebraic equations for equilibrium not only at t_n and t_{n+1} but also, additionally, in the RK-stages of time integration.

The advantage of the present methodology compared to the aforementioned one is, that it restricts the (global) finite element solutions for equilibrium to the ends of a time interval $\Delta t = t_{n+1} - t_n$. Making the solutions in the RK stages dispensable implies considerable compuational savings.

The difference between DAE/MLNA and the present framework can also be visualized in the schematic representation of Fig. 3 for the space-time coupling or global-local coupling. If, for example, a DIRK3 is used, the present methodology requires only one single, global equilibrium solution per time step. DAE/MLNA in contrast, requires 3 global finite element solutions at t_{ni}, $i = 1, 2, 3$ for the same time step. Therefore, we can expect for the same accuracy an approximate speed-up of the present approach by a factor of 3 (generally we expect for an s-stage method a speed-up factor of s if the last stage coincides with the end of the time interval) compared with DAE/MLNA.

Put different, the present approach can generate strain data at RK stages by interpolation, which are of the same quality in terms of their consistency order, as those strains in the DAE/MLNA approach satisfying equilibrium but for a fraction of the computational costs of the latter method.

Of course, the storage of total strain data for interpolation creates an additional computational overhead in the present approach, but it is far less time-consuming than additional solutions for global equilibrium in the RK stages.

5 Numerical examples

In this section, the performance of different DIRK schemes as listed in Table 3 is analyzed.

Table 2 Time integration algorithm for viscoelasticity using DIRK methods of order $p \in \{2, 3, 4\}$ along with a consistent total strain interpolation of order p

(I) Compute the start values $\boldsymbol{\Sigma}_{ni}$ for time integration (a_{ij}, c_j from Table 17 in the Appendix:

For $i = 1: \ \boldsymbol{\Sigma}^{\mathrm{v}}_{ni} = \boldsymbol{C}^{\mathrm{v}}_{n}$. For $i \geq 2: \ \boldsymbol{\Sigma}^{\mathrm{v}}_{ni} = \boldsymbol{C}^{\mathrm{v}}_{n} + \Delta t_n \sum_{j=1}^{i-1} a_{ij} \, \dot{\boldsymbol{C}}^{\mathrm{v}}_{nj}$ (49)

(II) Approximation of the total strain by polynomials of consistent degree $p-1$:

for $p \in \{2, 3, 4\}: \boldsymbol{C}_{ni} = \hat{\boldsymbol{C}}_{ni}(c_i, \boldsymbol{C}_{n+1}, \ldots, \boldsymbol{C}_{n-p+2})$ (50)

according to (41) for $p = 2$, (43) for $p = 3$, and (44) for $p = 4$.

(III) Compute the stage solutions $\boldsymbol{C}^{\mathrm{v}}_{ni}$:

$$\boldsymbol{C}^{\mathrm{v}}_{ni} = \boldsymbol{\Sigma}^{\mathrm{v}}_{ni} + \Delta t_n a_{ii} \, \dot{\boldsymbol{C}}^{\mathrm{v}}_{ni} \tag{51}$$

$$\text{with} \quad \dot{\boldsymbol{C}}^{\mathrm{v}}_{ni} = \frac{4\mu}{\eta} \frac{(\det \boldsymbol{C}^{\mathrm{v}}_{ni})^{1/3}}{(\det \boldsymbol{C}_{ni})^{1/3}} \left(\boldsymbol{C}_{ni} - \frac{1}{3} (\boldsymbol{C}_{ni} : \boldsymbol{C}^{\mathrm{v}-1}_{ni}) \boldsymbol{C}^{\mathrm{v}}_{ni} \right) \tag{52}$$

Solution of the nonlinear algebraic equations $\Phi_m = 0, m = 1, 2$, according to (30) and (31) for $x_i, i = 1, 2$ with $x_1 = \left(\det \boldsymbol{C}^{\mathrm{v}}_{ni}\right)^{1/3}$, $x_2 = \boldsymbol{C}_{ni} : \boldsymbol{C}^{\mathrm{v}-1}_{ni}$ yielding the stage solutions:

$$\boldsymbol{C}^{\mathrm{v}}_{ni} = \left[1 + \frac{\hat{k} x_1 x_2}{3\eta} \right]^{-1} \left[\boldsymbol{C}^{\mathrm{v}}_{ni-1} + \hat{k} \frac{x_1}{\eta} \right] \tag{53}$$

$$\text{with} \quad \hat{k} = \frac{4\mu \Delta t_n a_{ii}}{(\det \boldsymbol{C}_{ni})^{1/3}} \tag{54}$$

(IV) Compute the stage derivatives $\dot{\boldsymbol{C}}^{\mathrm{v}}_{ni}$:

$$\dot{\boldsymbol{C}}^{\mathrm{v}}_{ni} = \frac{\boldsymbol{C}^{\mathrm{v}}_{ni} - \boldsymbol{\Sigma}^{\mathrm{v}}_{ni}}{\Delta t_n a_{ii}} \tag{55}$$

If $i < s$ then $i = i + 1$, goto **(I)**, else continue

(V) Update viscoelastic strain $\boldsymbol{C}^{\mathrm{v}}_{n+1}$ and overstress $\boldsymbol{S}^{\mathrm{ov}}_{n+1}$:

$$\boldsymbol{C}^{\mathrm{v}}_{n+1} = \boldsymbol{C}^{\mathrm{v}}_{ns}$$

$$\boldsymbol{S}^{\mathrm{ov}}_{n+1} = 2\mu \frac{(\det \boldsymbol{C}^{\mathrm{v}}_{ns})^{1/3}}{(\det \boldsymbol{C}_{ns})^{1/3}} \left(\boldsymbol{C}^{\mathrm{v}-1}_{ns} - \frac{1}{3} (\boldsymbol{C}_{ns} : \boldsymbol{C}^{\mathrm{v}-1}_{ns}) \boldsymbol{C}^{-1}_{ns} \right) \tag{56}$$

The algorithm can be used within the *partitioned* solution framework for inelastic finite element computations, which requires equilibrium solutions only at t_n and t_{n+1} but not in the RK stages

Table 3 Different DIRK methods, their abbreviation, the number of stages s, the expected order in time integration $\min\{p, q\}$ versus the nominal order p, and the approximation order of total strain q

Method/abbreviation	No. of stages s	$\min\{p, q\}$	vs.	p	q	Strain approx
DIRK1/BE	1	*1*	=	*1*	***p***	constant
DIRK2l	2	*2*	=	*2*	***p***	linear
DIRK3cons	3	1	<	3	$p-2$	constant
DIRK3l	3	2	<	3	$p-1$	linear
DIRK3q	3	*3*	=	*3*	***p***	quadratic
DIRK4c	5	*4*	=	*4*	***p***	cubic

The methods with consistent strain interpolation are italicised

Table 3 reflects one of the main statements of the present work. A time integration method of a nominal order p requires a consistent approximation of the total strain tensor $\boldsymbol{C}(t)$ of order $q = p$ to obtain full order of convergence. DIRK methods, which conceptually fulfil this requirement, are italicised in Table 3. If, however, strain interpolation of the order $p - m$ with $m \geq 1$ is used, then order reduction to the reduced order $p - m$ must be expected.

The main focus is on the following aspects:

1. *Convergence order* Measuring the convergence order checks the validity of the novel, generalized concept. The convergence order is calculated for the total strain tensor $\boldsymbol{C}$ as a *primary* unknown (note that $\boldsymbol{C}$ and $\boldsymbol{u}$ have the same order in time) and for quantities following from time integration like viscoelastic strain $\boldsymbol{C}^{\mathrm{v}}$ and stress $\boldsymbol{S}^{\mathrm{ov}}$. Consequently, an accurate reference solution $\boldsymbol{X}^{\mathrm{ex}}$ for tensor $\boldsymbol{X}$ with $\boldsymbol{X} = \{\boldsymbol{C}, \boldsymbol{C}^{\mathrm{v}}, \boldsymbol{S}^{\mathrm{ov}}\}$ is calculated by *numerical overkill* using a very small time step size where the accuracy of the results is in the range of machine precision. Based on this reference solution, a relative, global error for finite time step sizes is calculated according to

$$e(\boldsymbol{X}) = \frac{1}{N_{\mathrm{el}} \cdot N_{\mathrm{gauss}}} \sum_{i=1}^{N_{\mathrm{el}}} \sum_{j=1}^{N_{\mathrm{gauss}}} \frac{||\boldsymbol{X}^{(ij)}(\Delta t) - \boldsymbol{X}^{(ij)\mathrm{ex}}||}{||\boldsymbol{X}^{(ij)\mathrm{ex}}||} , \tag{57}$$

where $\boldsymbol{X}^{(ij)}(\Delta t)$ is the result for a time step size Δt, N_{el} is the number of elements in the domain and N_{gauss} is the number of Gauss-points per element.
In the following, the relative error versus the time step size Δt is displayed in doubled logarithmic scaling. The mean order of convergence is calculated by means of linear regression, if convergence is uniform.

Table 4 Radial contraction of an annulus: viscoelastic material parameters

c_{01} (N/mm^2)	c_{10} (N/mm^2)	c_{30} (N/mm^2)	K (N/mm^2)	μ (N/mm^2)	η_0 (N s/mm^2)
0.5	0.264	0.19	1000.0	0.2	200.0

Note, that uniform convergence will only show up, if the time step size is constant. This is the reason why we abaondon—here—the attractive option for varying time step sizes within an adaptive solution strategy[3].

2. *Efficiency* The efficiency is measured in terms of the error as a function of the overall computation time. This test will provide a fair comparison of different time integration schemes. Moreover, the actual speed-up of different methods compared with BE is measured for a prescribed global error tolerance.
   Note, that taking only fixed time step sizes into account neatly separates the improved efficiency of higher-order RK methods by virtue of the present space-time coupling concept from the additional benefit of embedded RK methods to enable higher efficiency via adaptivity.
3. *Reliability* In order to achieve reliable conclusions concerning the performance of the time integrators, the simulations are carried out for different test sets. In [9] it is observed, that time integration methods perform much better in test sets with uniform deformations (like simple shear or biaxial tension) compared with inhomogeneous deformation states. For that reason we consider the following sets of simulations:

   (a) Radial contraction of an annulus. Material Parameters according to Table 4.
   (b) Quadratic plate with a hole subject to (i) linearly increasing, tensile load, (ii) sinusoidal loading, and (iii) superposition of (i) and (ii). Material Parameters according to Table 4.
   (c) Variation of material parameters for the set (b). The isochoric case is considered by setting $\nu = 0.499239$. In a second set of material parameters, the isochoric constraint is relaxed to $\nu = 0.33$.
   The Poisson contraction follows from the relation, cf. [22],

$$\nu = \frac{3K - 4(c_{10} + c_{01})}{6K + 2(c_{10} + c_{01})} \tag{58}$$

   where for the case $\nu = 0.33$ the compression modulus K is changed, and all other material parameters $c_{10}, c_{01}, c_{30}, \eta$ of Table 4 are held fixed.

The DIRK schemes along with the finite strain viscoelasticity model of Sect. 2.2 have been implemented into an extended version of the finite element code FEAP, [42]. The finite element that is used in the simulations is a Q1P0 element.

Remark Since the total strain calculation has the characteristic of a multistep method for $p \geq 3$ (i.e. at least quadratic strain interpolation), it requires a starting procedure. In the first time step, linear interpolation of total strain (hence $q = 2$) is the most accurate approximation that can be obtained. As a consequence, for $p \geq 3$ the condition $q = p$ is necessarily violated in the very first time interval. For e.g. the 4th-order DIRK method total strain data from 4 points $t_{n-2}, t_{n-1}, t_n, t_{n+1}$ are necessary for calibrating a polynomial of degree 3. These data, however, are available not earlier than in the 3rd overall time step. As a consequence, "under-interpolation" must be used in the first two time steps using linear, then quadratic strain interpolation.

We anticipate already here, that this necessarily inconsistent starting procedure has no negative effect on the convergence order of time integration.

5.1 Radial contraction of an annulus

In the first test set we consider the radial contraction of an annulus, which exhibits radii $r_i = 20\,\text{mm}$, $r_o = 40\,\text{mm}$ and thickness $t = 1\,\text{mm}$ as displayed in Fig. 4. Two sym-

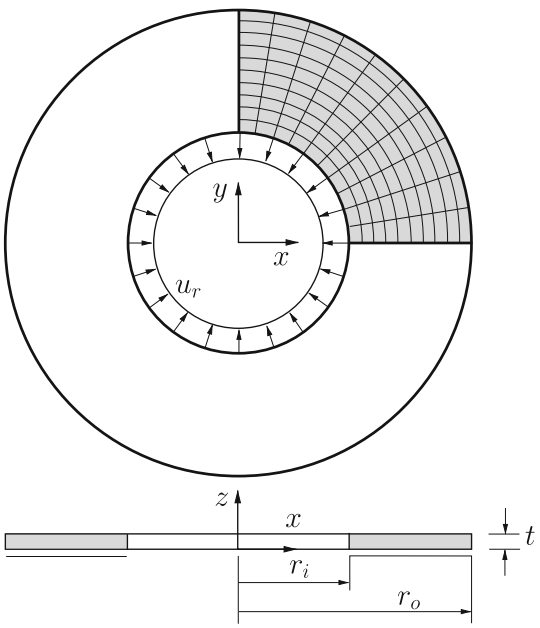

Fig. 4 Radial contraction of a viscoelastic annulus by displacement control applied to the inner rim: geometry, loading, and the finite element mesh of the quarter system.

[3] Embedded RK methods provide an error estimate and therefore enable an automatic step-size control.

Table 5 Radial contraction of an annulus: order of convergence for different DIRK methods

Time $t = 1.5$ s Error	$e(\boldsymbol{C})$	$e(\boldsymbol{C}^{\mathrm{v}})$	$e(\boldsymbol{S}^{\mathrm{ov}})$	$e(\boldsymbol{S})$
BE	1.01	1.00	1.00	1.00
DIRK2l	*1.94*	*1.93*	*1.93*	*1.94*
DIRK3cons	1.01	1.00	1.00	1.00
DIRK3l	2.14	1.76	1.73	1.94
DIRK3q	*2.82*	*2.96*	*2.95*	*2.91*
DIRK4q	2.82	2.96	2.95	2.91
DIRK4c	*2.80*	*2.93*	*2.93*	*2.89*

The results for consistent strain approximation are italicised

metry planes are exploited in the simulation, such that the simulation is performed at a quarter system. The plate is supported in z-direction at $z = 0$. As shown in Fig. 4, the quarter system is discretized by 10 elements in circumferential direction, 10 elements in radial direction and one element over the thickness.

Starting from $t = 0$ s the inner rim is continuously pulled inwards in radial direction by displacement control up to a total displacement of $u_r = 1.5$ mm at $t = 1.5$ s, hence $u_r(t) = 1\text{mm/s} \cdot t$. The time step sizes are $\Delta t = \{0.025, 0.05, 0.075, 0.1, 0.125, 0.25\}$s. The reference solution is calculated by DIRK4c using a time step size of Δt =1.0E-04 s.

Results and discussion The convergence behavior is documented in Table 5 and in the diagrams of Fig. 5. It reveals that the 3rd order DIRK3 obtains full convergence order only for a quadratic, hence consistent interpolation of total strain (DIRK3q). Linear strain interpolation (DIRK3l) in contrast, induces a local approximation error for total strains of order 2, which propagates to an order reduction to order 2. In line with the previous results is the order reduction to order 1, if total strains are held constant (DIRK3cons) in the time interval, here $\boldsymbol{C}(t) := \boldsymbol{C}_{n+1}$.

The simulation results are in agreement with the order considerations in Sect. 4; the approximation order in time of the total strain tensor $\boldsymbol{C}(t)$ is (approximately) an upper bound for the convergence order of $\boldsymbol{C}^{\mathrm{v}}$, $\boldsymbol{S}^{\mathrm{ov}}$ and $\boldsymbol{S}$.

The only result which seems not to fit to our predictions is the fact that DIRK4c shows convergence order 3, although cubic strain interpolation is employed. In the next test set we will introduce a pronounced nonlinearity via sinusoidal load-

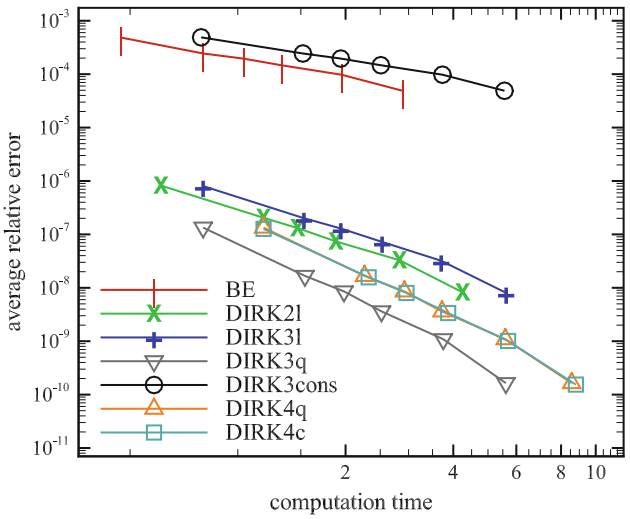

Fig. 6 Radial contraction of an annulus: efficiency for linearly increasing load in terms of the overall error $e(\boldsymbol{S})$ vs. the computation time (s) for evaluations at time $t = 1.5$ s.

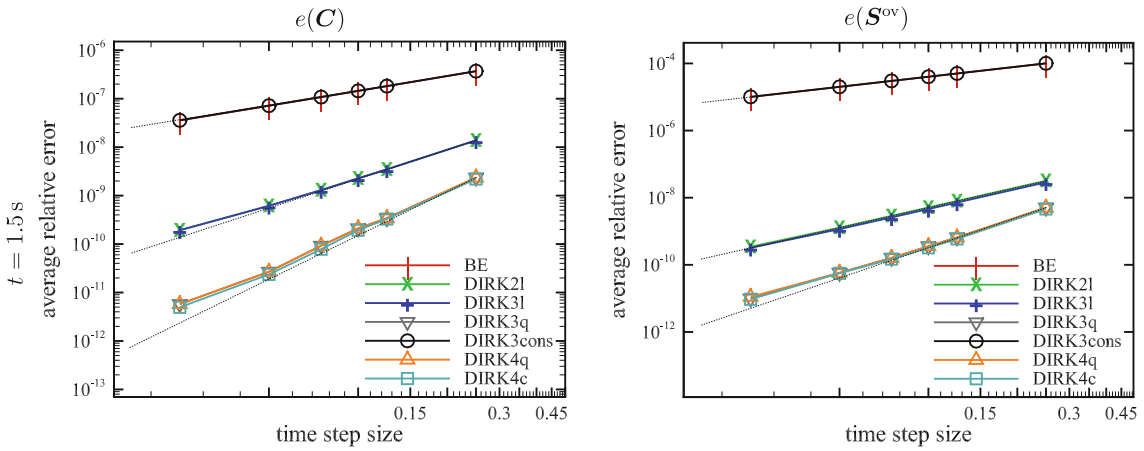

Fig. 5 Radial contraction of an annulus: error versus time step-size evaluated at $t = 1.5$ s for different time integrators. *Left* $e(\boldsymbol{C})$, *right* $e(\boldsymbol{S}^{\mathrm{ov}})$.

Table 6 Radial contraction of an annulus: speed-up factors of DIRK methods compared with BE for different error tolerances

	Speed-up factor	
Error tol. $e(\boldsymbol{S}^{\mathrm{ov}})$	1.0E−04	1.0E−06
BE	1.0	1.0
DIRK2l	31.7	250.3
DIRK3cons	0.5	0.5
DIRK3q	19.0	327.8
DIRK4c	13.6	225.7

Error calculations for $e(\boldsymbol{S}^{\mathrm{ov}})$ are carried out at time $t = 1.5\,\mathrm{s}$

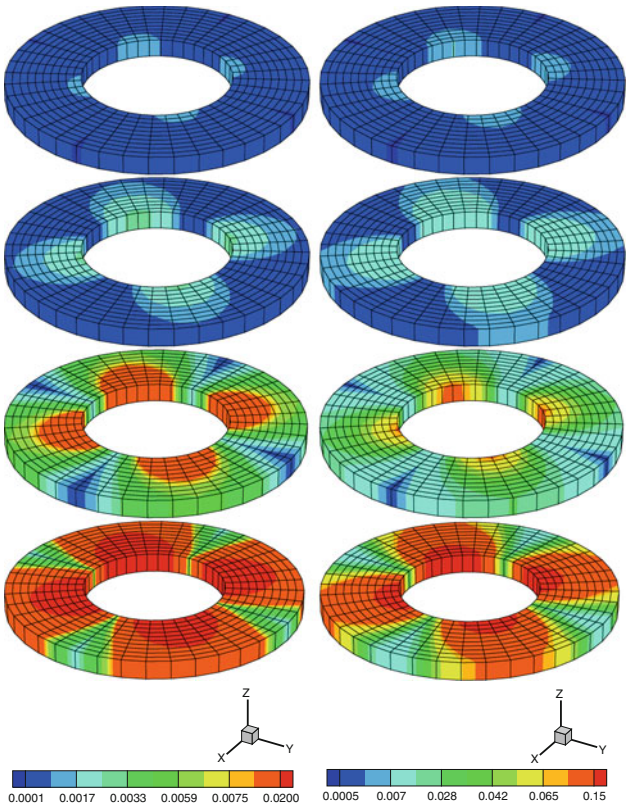

Fig. 7 Radial contraction of an annulus at $t = \{0.5, 1.0, 5.0, 15.0\}\,\mathrm{s}$ from top to bottom. *Left* overstress component $S^{\mathrm{ov}}_{xy}\,(\mathrm{N/mm^2})$. *Right* total stress component $S_{xy}\,(\mathrm{N/mm^2})$

ing in time instead of the linearly increasing load as chosen here.

Figure 5 shows, that all DIRK methods with consistent strain approximation significantly excel the convergence order of BE. For a fair comparison of the methods we measure their efficiency in terms of the error in stress versus the overall computation time. As a result, higher order DIRK methods are much more efficient than BE. Figure 6 reveals, that DIRK3q is for small error tolerances the most efficient method. Since the convergence order seems to be limited in this particular example to order 3, DIRK4c cannot excel DIRK3q; it shows the same convergence order as DIRK3q but exhibits two more stages (5 instead of 3) and therefore it is less efficient than DIRK3q.

The improvement in efficiency is measured by speed-up factors shown in Table 6; DIRK2l is the winner with a speed-up of more than factor 30 compared with BE for an error tolerance of $1.0E-04$. DIRK4c and DIRK3q show speed-up factors of 13.6 and 19, respectively. The speed-up becomes much more pronounced for smaller error tolerances. Speed-up factors well above 200 are obtained by all DIRK variants for an error tolerance of $1.0E-06$.

If DIRK3 is used along with a total strain held constant in the time interval, $\boldsymbol{C}(t) := \boldsymbol{C}_{n+1}$, then the results are the worst. Since the convergence order falls back to order 1 and the computational effort is for this 3-stage method much larger than for BE, the overall performance is even worse than BE, see Fig. 6 and Table 6.

The deformation of the annulus at different stages is displayed in Fig. 7.

5.2 Quadratic plate with a hole

5.2.1 Linearly increasing load

In the present example we consider the stretch of a quadratic plate with a hole, see Fig. 8. The geometry of the structure is given by length $l = 100\,\mathrm{mm}$ and thickness $t = 2\,\mathrm{mm}$. The plate exhibits a hole of radius $r = 3\,\mathrm{mm}$.

Starting at $t = 0\,\mathrm{s}$ the plate is stretched by linearly increasing displacements up to a total displacement of $u = 15\mathrm{mm}$ at $t = 1.5\,\mathrm{s}$ at two opposite edges, hence $u(t) = 10\mathrm{mm/s} \cdot t$.

The strip is supported in its midsurface in thickness-direction, and supported orthogonal to the symmetry planes in width direction and in length direction, respectively. Exploiting three symmetry planes allows for a simulation

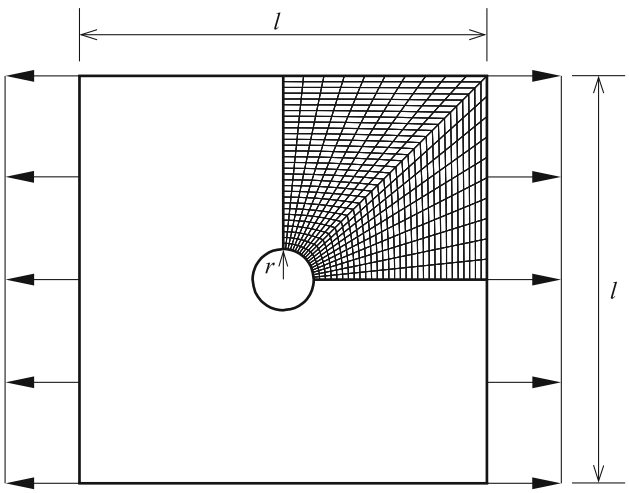

Fig. 8 FE-model of the quadratic plate with a hole; geometry, loading, discretization of one eighth using symmetries.

Table 7 Quadratic plate with a hole for linearly increasing load: order of convergence of different quantities for variants of DIRK methods

Time $t = 1.5$ s Error	$e(\boldsymbol{C})$	$e(\boldsymbol{C}^{\mathrm{v}})$	$e(\boldsymbol{S}^{\mathrm{ov}})$	$e(\boldsymbol{S})$
BE	1.00	1.00	1.00	1.00
DIRK2l	*1.78*	*1.56*	*1.91*	*1.73*
DIRK3cons	1.00	1.00	1.00	1.00
DIRK3l	1.78	1.55	1.91	1.69
DIRK3q	*2.61*	*2.50*	*2.94*	*2.72*
DIRK4q	2.61	2.50	2.94	2.67
DIRK4c	*2.69*	*2.47*	*2.94*	*2.67*

The results for consistent strain approximation are italicised

of one eighth system, the resulting structure is discretized by $30 \times 10 \times 2$ elements, see Fig. 8.

The same viscoelastic material parameters as in the previous example are used, see Table 4. Time step sizes considered in the simulations are $\Delta t = \{0.025, 0.05, 0.075, 0.1, 0.125, 0.25\}$s, the reference values are calculated using DIRK4c along with Δt =1.0E-04 s.

Results and discussion The analysis of the convergence order is summarized in Table 7 and in the diagrams of Fig. 9. It can be observed that DIRK3 is of order 3, if strain interpolation is quadratic. Similarly, DIRK2 is of order 2, if strain interpolation is linear. This underpins the rationale of the present work, that time integration of order p requires an approximation of total strains of the same order p. If polynomials of lower order $q < p$ are used, then the approximation order of total strain $\boldsymbol{C}$ is an upper bound for the convergence order of viscoelastic strain $\boldsymbol{C}^{\mathrm{v}}$ and for total stress $\boldsymbol{S}^{\mathrm{ov}}$, respectively. This case is called *order reduction*. In line with the previous results is the order reduction to order 1, if total strains are held constant (DIRK3cons).

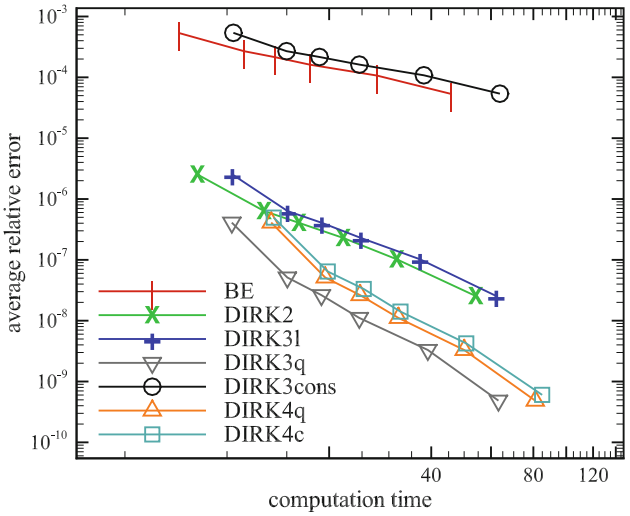

Fig. 10 Quadratic plate with a hole for linearly increasing load: efficiency in terms of the overall error $e(\boldsymbol{S}^{\mathrm{ov}})$ versus the overall computation time (s) at time $t = 1.5$ s.

Remarkably, DIRK4c shows again not more than convergence order 3. The obtained order 2.7 for total strains indicates, that cubic polynomials are not superior to quadratic polynomials for total strain interpolation in this particular problem. In the next test set we will see that a more pronounced nonlinearity in the loading can change the convergence order.

Figure 9 shows that all DIRK methods with consistent strain approximation significantly improve the convergence order of BE. The efficiency of the methods is measured in terms of the error in the overstress versus the overall computation time, see Fig. 10.

Table 8 reveals, that for an error tolerance of 1.0E-04 a relation for the speed-up factors holds according to 11.8 (DIRK2l) > 7.6 (DIRK3q) > 5.5 (DIRK4c). This

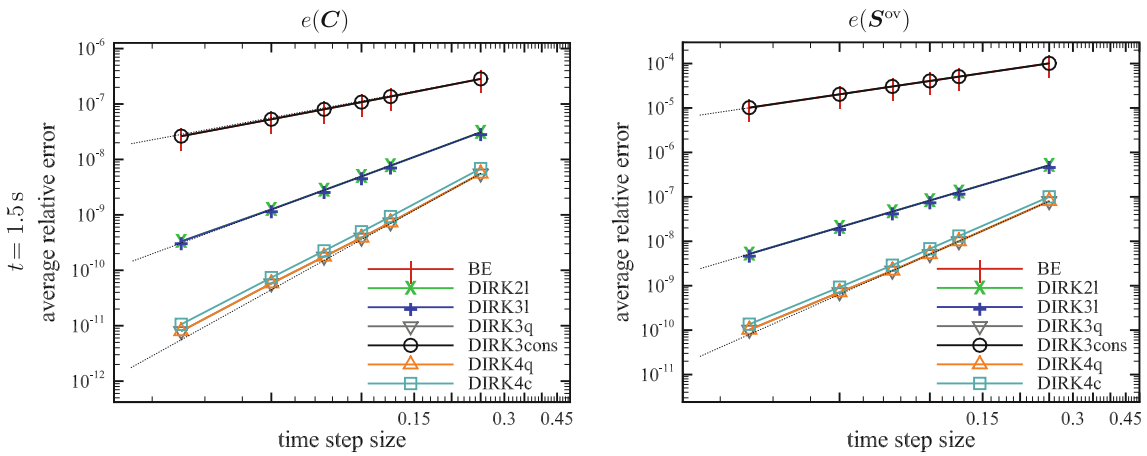

Fig. 9 Quadratic plate with a hole for linearly increasing load: error versus time step size evaluated at $t = 1.5$ s for different time integrators. *Left* $e(\boldsymbol{C})$, *right* $e(\boldsymbol{S}^{\mathrm{ov}})$.

Table 8 Quadratic plate with a hole for linearly increasing load: speed-up factors of DIRK methods compared with BE for different error tolerances

Error calculations are carried out at time $t = 1.5\,\mathrm{s}$ for $e(\boldsymbol{S}^{\mathrm{ov}})$

	speed-up factor	
Error tol. $e(\boldsymbol{S}^{\mathrm{ov}})$	1.0E-04	1.0E-06
BE	1.0	1.0
DIRK2l	11.8	179.2
DIRK3cons	0.7	0.7
DIRK3q	7.6	226.2
DIRK4c	5.5	164.3

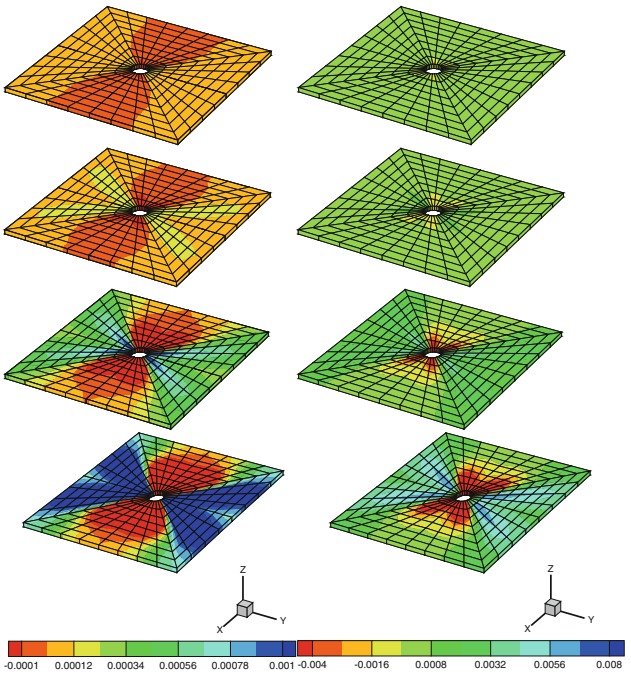

Fig. 11 Quadratic plate with a hole for linearly increasing load at $t = \{0.5, 1.0, 5.0, 15.0\}\,\mathrm{s}$ from top to bottom. *Left* overstress component S^{ov}_{xy} $(\mathrm{N/mm^2})$. *Right* total stress component S_{xy} $(\mathrm{N/mm^2})$

relation indicates, that here, the increasing computational complexity due to more stages is predominant for the performance of the method. Notwithstanding, all methods show a speed-up beyond factor 5 compared with BE. For a smaller error tolerance of 1.0E-06, the higher order of DIRK3q leads to a superior speed-up compared with DIRK2l. DIRK4c is still behind DIRK2l due to its higher numerical effort of 5 stages instead of 2. But all higher order DIRK methods show for this error tolerance a drastic speed-up in the range of 164–226 compared with BE. The deformed plate at different stages is shown in Fig. 11.

5.2.2 *Sinusoidal loading—incompressible material parameters*

Next, we replace for the same setting as in Sect. 5.2.1 the linearly increasing load by a sinusoidal load of the form

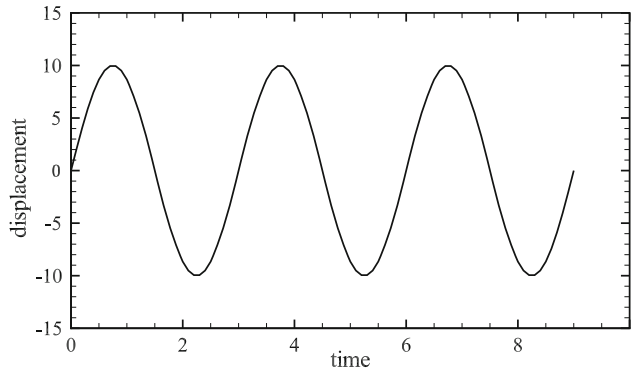

Fig. 12 Sinusoidal loading in time

$u(t) = 10\,\mathrm{mm/s} \cdot \sin(2/3\pi t)$, see Fig. 12. This kind of loading introduces a stronger nonlinearity in the strain path compared with a loading that linearly increases.

The reference solution is calculated using DIRK4c with a time step size of $\Delta t = 0.0001\,\mathrm{s}$, for error calculations step size is between $\Delta t = 0.003125\,\mathrm{s}$ and $\Delta t = 0.125\,\mathrm{s}$.

Results and discussion The convergence results are shown in Fig. 13 and in Table 9. In contrast to the previous setting, the convergence order of $\boldsymbol{C}^{\mathrm{v}}$, $\boldsymbol{S}^{\mathrm{ov}}$ and $\boldsymbol{S}$ for DIRK4c is well above 3 but still below 4. It is much better for cubic strain interpolation than for quadratic interpolation.

Similarly, all other methods show the predicted convergence behavior as summarized in Table 3. Furthermore, as in the previous examples, all quantities $\boldsymbol{C}$, $\boldsymbol{C}^{\mathrm{v}}$, $\boldsymbol{S}^{\mathrm{ov}}$ and $\boldsymbol{S}$ show approximately the same error patterns, see Table 9.

The diagram in Fig. 14 displays the numerical efficiency in terms of the error in the overstress versus the overall computation time.

Table 10 gives explicit numbers for the speed-up in computation of higher order DIRK methods compared with BE. The speed-up for an error tolerance of 1.0E-04 (1.0E-06, respectively) is considerable and throughout in the range of factor 5 (factors 25–53 respectively) for the DIRK methods with $p \geq 2$.

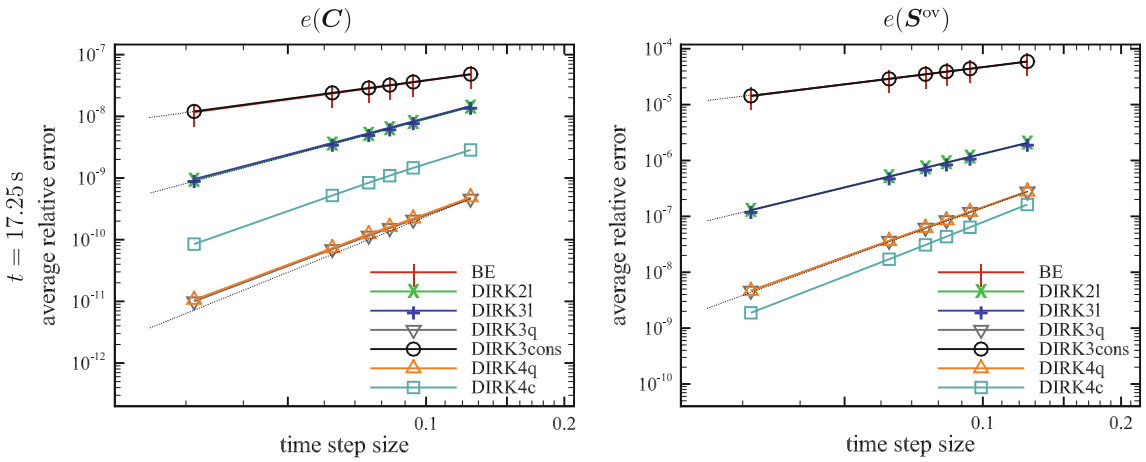

Fig. 13 Quadratic plate with a hole for sinusoidal loading and incompressible viscoelasticity: error versus time step size evaluated at $t = 17.25\,\mathrm{s}$ for different DIRK methods. *Left* $e(\boldsymbol{C})$, *right* $e(\boldsymbol{S}^{\mathrm{ov}})$.

Table 9 Quadratic plate with a hole for sinusoidal loading and incompressible viscoelasticity: order of convergence for different methods

Error	$e(\boldsymbol{C})$		$e(\boldsymbol{C}^{\mathrm{v}})$		$e(\boldsymbol{S}^{\mathrm{ov}})$		$e(\boldsymbol{S})$	
Time t	8.25 s	17.25 s	8.75 s	17.25 s	8.25 s	17.25 s	8.25 s	17.25 s
BE	1.00	1.01	1.01	1.01	1.01	1.01	1.01	1.01
DIRK2l	*1.92*	*1.89*	*2.00*	*2.00*	*2.00*	*2.00*	*2.00*	*2.00*
DIRK3cons	0.99	1.00	1.01	1.01	1.01	1.01	1.01	1.01
DIRK3l	1.93	1.89	2.00	2.00	2.00	2.00	2.00	2.00
DIRK3q	*2.83*	*2.61*	*2.91*	*2.90*	*2.94*	*2.95*	*2.94*	*2.95*
DIRK4q	2.72	2.61	2.91	2.90	2.94	2.95	2.94	2.95
DIRK4c	*2.49*	*2.50*	*3.24*	*3.24*	*3.23*	*3.23*	*3.24*	*3.24*

The methods with consistent strain interpolation are italicised

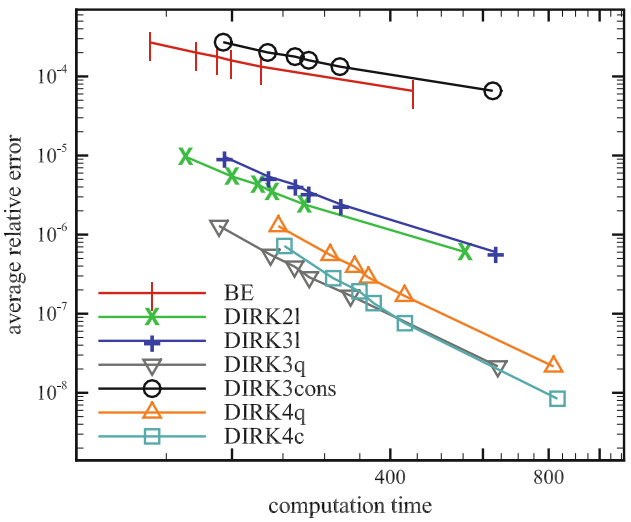

Fig. 14 Quadratic plate with a hole for sinusoidal loading and incompressible viscoelasticity: efficiency in terms of the error $e(\boldsymbol{S}^{\mathrm{ov}})$ vs. the computation time (s) for evaluations at $t = 8.25\,\mathrm{s}$.

Table 10 Quadratic plate with a hole for sinusoidal loading and incompressible viscoelasticity: speed-up factors of different methods compared with BE for different error tolerances

	Speed-up factor	
Error tol. $e(\boldsymbol{S}^{\mathrm{ov}})$	1.0E−04	1.0E−06
BE	1.0	1.0
DIRK2l	4.4	25.0
DIRK3cons	0.7	0.7
DIRK3q	5.4	52.8
DIRK4c	3.8	46.0

Error calculations at time $t = 8.25\,\mathrm{s}$

5.2.3 Sinusoidal loading—compressible material behavior

Next, we study the influence of a supposedly minor change in the material parameters. The compression modulus is set to $K = 3\ \mathrm{N/mm^2}$, which implies according to (58) a Poisson

Table 11 Quadratic plate with a hole for sinusoidal loading and compressible viscoelasticity, $\nu = 0.3$: order of convergence for different methods

Error	$e(\boldsymbol{C})$		$e(\boldsymbol{C}^{\mathrm{v}})$		$e(\boldsymbol{S}^{\mathrm{ov}})$	
Time t	8.25 s	17.25 s	8.75 s	17.25 s	8.25 s	17.25 s
BE	1.02	1.02	1.02	1.02	1.02	1.02
DIRK2l	*2.00*	*2.00*	*2.00*	*2.00*	*2.00*	*2.00*
DIRK3cons	1.02	1.02	1.02	1.02	1.02	1.02
DIRK3l	2.00	2.00	2.00	2.00	2.00	2.00
DIRK3q	*2.67*	*2.68*	*2.94*	*2.95*	*2.95*	*2.95*
DIRK4q	2.67	2.68	2.94	2.94	2.94	2.95
DIRK4c	*3.03*	*2.98*	*3.58*	*3.58*	*3.64*	*3.64*

The methods with consistent strain interpolation are italicised

contraction of $\nu = 0.3$. Hence, we considerably relax the constraint of quasi-incompressibility.

Results and discussion Concerning the simulation results we restrict to the differences to the quasi-incompressible case. For the present case, cubic polynomials turn out to be much better for strain interpolation than quadratic polynomials, which manifests in the convergence orders of $e(\boldsymbol{C})$ in Table 11 for DIRK4c and for DIRK4q. As a consequence, quantities from viscoelastic time integration, i.e. $\boldsymbol{C}^{\mathrm{v}}$ and $\boldsymbol{S}^{\mathrm{ov}}$ exhibit convergence order of approx. 3.6 for DIRK4c which is clearly above the observed order (≈3.24 in Table 11) in the quasi-incompressible case (Fig. 15).

The diagram in Fig. 16 shows the numerical efficiency in terms of the error in overstress versus the computation time. Remarkably, DIRK4c can overpower its drawback as an expensive 5-stage method compared with the 3-stage method DIRK3q by virtue of its higher convergence order; for small error tolerances it is the fastest method.

Table 12 gives explicit numbers for the speed-up in computation of higher order DIRK methods compared with BE. The speed-up is considerable and throughout above factor 4 for all DIRK methods with $p \geq 2$ if an error tolerance of 1.0E-04 is set.

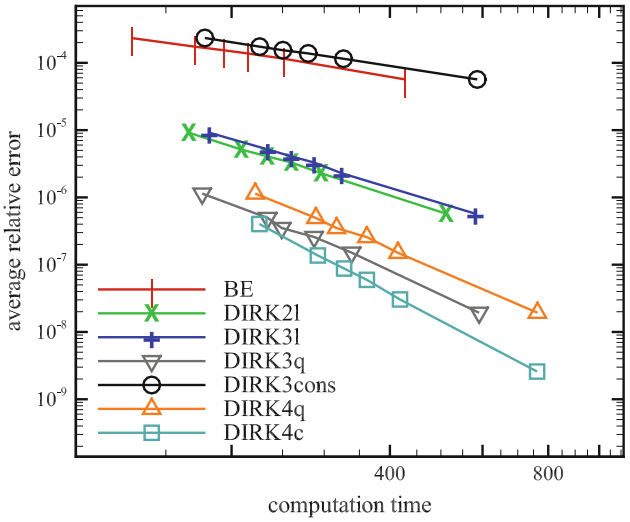

Fig. 16 Quadratic plate with a hole for sinusoidal loading and compressible viscoelasticity, $\nu = 0.3$: efficiency in terms of the error $e(\boldsymbol{S}^{\mathrm{ov}})$ vs. the computation time (s) for evaluations at $t = 8.25$ s.

Table 12 Quadratic plate with a hole for sinusoidal loading and compressible viscoelasticity: speed-up factors of different methods compared with BE for different error tolerances

	speed-up factor	
error tol. $e(\boldsymbol{S}^{\mathrm{ov}})$	1.0E-04	1.0E-06
BE	1.0	1.0
DIRK2l	4.4	21.6
DIRK3cons	0.8	0.5
DIRK3q	7.3	48.1
DIRK4c	4.6	48.7

Error calculations at time $t = 8.25$ s

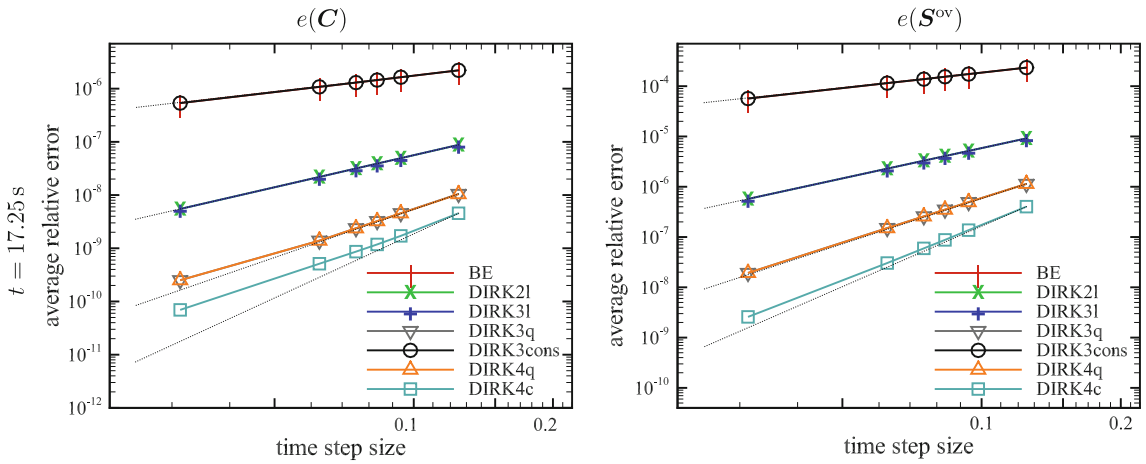

Fig. 15 Quadratic plate with a hole for sinusoidal loading and compressible viscoelasticity: error versus time step size evaluated at $t = 8.25$ s for different DIRK methods. *Left* $e(\boldsymbol{C})$, *right* $e(\boldsymbol{S}^{\mathrm{ov}})$.

5.2.4 *Superposition of linearly increasing load with sinusoidal fluctuations*

Next, we consider the superposition of a linearly increasing and a sinusoidal loading as visualized in Fig. 17. The loading is mediated by displacement control according to

$$u(t) = 10\,(\mathrm{mm/s}) \cdot t + 20\,(\mathrm{mm/s}) \cdot \sin\left(\frac{2}{3}\pi t\right). \tag{59}$$

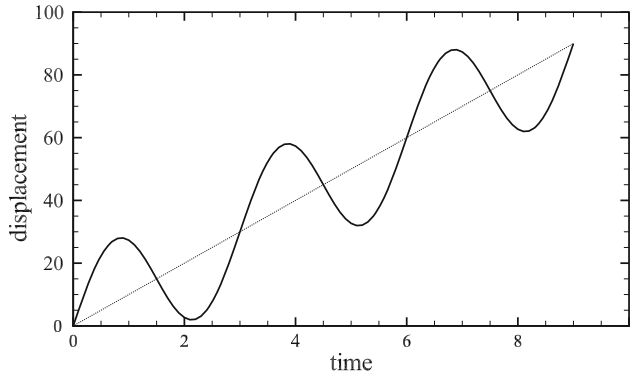

Fig. 17 Superposition of linearly increasing loading with sinusoidal fluctuations in time

The material parameters are taken from Table 4 (i.e. the quasi-incompressible case).

The reference solution was calculated using DIRK4c with a time step size of Δt =1.0E-04 s.

Results and discussion The convergence results are shown in Fig. 18 and in Table 13. Again, all DIRK methods achieve full convergence order for consistent strain interpolation. Table 13 reveals that the approximation order for $\boldsymbol{C}$ is an upper bound for the convergence order $\boldsymbol{C}^{\mathrm{v}}$ and $\boldsymbol{S}^{\mathrm{ov}}$ in that order reduction is observed for strain interpolation of inconsistent order $p - m, m \geq 1$. As predicted by theory, this equally applies for DIRK3cons, DIRK3l and for DIRK4q.

Figure 19 shows the numerical efficiency in terms of the error in overstress versus the overall computation time. It reveals that all DIRK methods with $p \geq 2$ excel BE by a speed-up of at least a factor 15, see Table 14. Here, the speed-up of DIRK4c is due to its numerical costs as a 5-stage method smaller than the speed-up of the 3-stage method DIRK3q, which holds for an error tolerance of 1.0E-04. For an error tolerance of 1.0E-06 all DIRK methods with $p \geq 2$ yield a drastic speed-up with factors 127–232 compared with BE.

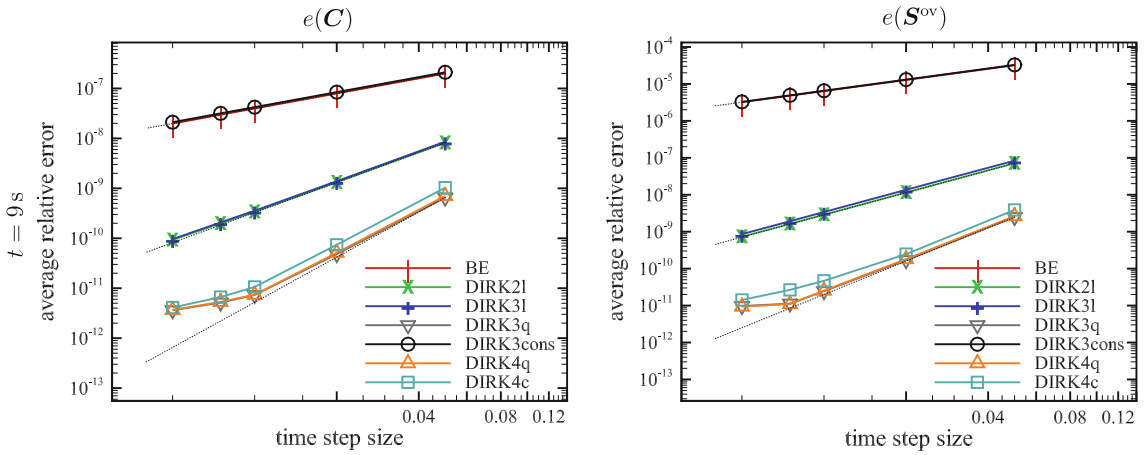

Fig. 18 Quadratic plate with a hole for superposition of linearly increasing loading with sinusoidal fluctuations: error versus time step size evaluated at $t = 9.0$ s for different DIRK methods. *Left* $e(\boldsymbol{C})$, *right* $e(\boldsymbol{S}^{\mathrm{ov}})$

Table 13 Quadratic plate with a hole for superposition of linearly increasing and sinusoidal loading: order of convergence for different methods

error	$e(\boldsymbol{C})$		$e(\boldsymbol{C}^{\mathrm{v}})$		$e(\boldsymbol{S}^{\mathrm{ov}})$		$e(\boldsymbol{S})$	
time t	3 s	9 s	3 s	9 s	3 s	9 s	3 s	9 s
BE	1.01	1.00	1.00	1.00	1.00	1.00	1.00	1.00
DIRK2l	*1.92*	*1.95*	*2.00*	*2.00*	*2.00*	*1.99*	*1.99*	*1.99*
DIRK3cons	1.01	1.00	1.00	1.00	1.00	1.00	1.00	1.00
DIRK3l	1.92	1.95	2.00	2.00	2.00	1.99	1.99	1.99
DIRK3q	*2.42*	*2.35*	*2.86*	*2.75*	*2.79*	*2.85*	*2.80*	*2.55*
DIRK4q	2.43	2.38	2.85	2.76	2.79	2.84	2.79	2.59
DIRK4c	*2.61*	*2.44*	*2.90*	*2.86*	*2.80*	*2.67*	*2.86*	*2.46*

The methods with consistent strain interpolation are italicised

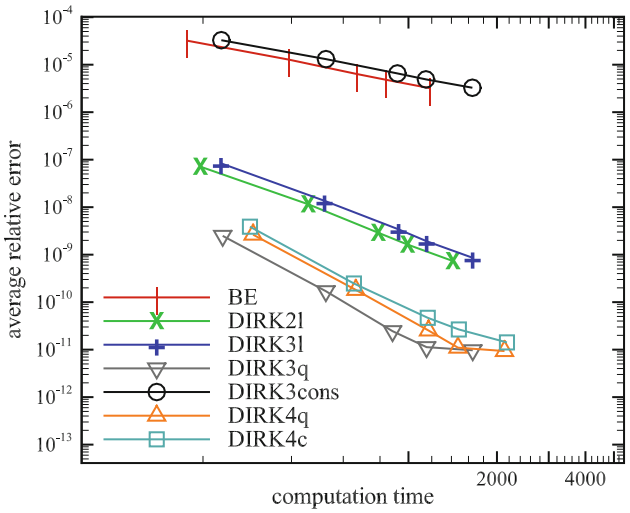

Fig. 19 Quadratic plate with a hole for superposition of linearly increasing and sinusoidal loading: efficiency in terms of the error $e(\boldsymbol{S}^{\mathrm{ov}})$ vs. the total computation time (s) for evaluations at $t = 9\,\mathrm{s}$.

Table 14 Quadratic plate with a hole for superposition of linearly increasing and sinusoidal loading: speed-up factor of DIRK methods compared with BE for different error tolerances

	speed-up factor	
error tol. $e(\boldsymbol{S}^{\mathrm{ov}})$	1.0E-04	1.0E-06
BE	1.0	1.0
DIRK2l	23.6	127.0
DIRK3cons	0.7	0.6
DIRK3q	19.5	232.3
DIRK4c	15.2	186.1

Error calculations at time $t = 9\,\mathrm{s}$

6 Summary and conclusions

In this paper we proposed a unified theoretical concept, which guarantees full convergence order $p \geq 2$ of RK-methods as time integrators for viscoelastic models in finite element analyses. Here, we have shown the validity of the concept for a fully-fledged finite-strain viscoelastic model. The key aspect is that strain-interpolation in time must be consistent with the order of convergence of the time integrator.

The main results shall be summarized.

1. RK methods of order p require for full convergence order an approximation of the total strain via interpolation of a consistent order p. Interpolation is carried out by polynomials of degree $p-1$ based on p collocation points, which are chosen to be at $t_{n+1}, t_n, \ldots, t_{n-(p-2)}$, $p \geq 2$. In agreement with the theoretical predictions in [9], order reduction inevitably occurs, if total strain interpolation is of an order less than p. If interpolation is of the order $p-m, m \geq 1$, then the order of time integration falls back to $p-m$. Hence, the order of strain interpolation is an upper bound for the convergence order in time integration.
2. The concept of consistent strain interpolation allows to preserve the partitioned ansatz of FEM for solving inelastic problems. Opposed to the DAE/MLNA concept in [12,20], global equilibrium solutions are not required at RK stages, which implies considerable computational savings.
3. The concept applies for arbitrary RK methods. DIRK methods are particularly efficient, since the RK stage solutions are decoupled. Hence, for a method with s stages, the solution is a sequence of s solution steps which can be treated each as BE.
4. Following the novel concept, the adapted RK time integrators obtain full convergence order in representative examples and thus approve the concept of consistent strain interpolation for a finite-strain viscoelastic model to full extent. Compared with BE, a considerable gain in efficiency for the same accuracy can be achieved.

In conclusion, the use of the novel concept of consistent strain interpolation for higher order RK (most notably DIRK) methods enables a considerable speed-up of viscoelastic finite element analyses. In view of its performance, relative ease in implementation and handling, the present framework can be unconditionally recommended.

Acknowledgments BE thanks DFG for financial support through the Heisenberg programme (grant no. EI 453/2-1) and acknowledges support from Mathematisches Forschungsinstitut Oberwolfach for participation in the workshop Advanced Computational Engineering in Feb. 2012. FS acknowledges financial support from Brazilian National Council for Scientific and Technological Development (CNPq) through the doctorate scholarship program under process number 290064/2010-4, which enabled his stay in Essen.

Appendix: Time integration using RK methods

Basic equations

To put things into perspective, we briefly recall some basic equations for the solution of an IVP by implicit RK (IRK) methods, cf. e.g. [17–19]. The IVP exhibits the format

$$\dot{z} = \boldsymbol{f}(z)\,, \qquad z(t_0) = z_0\,, \qquad t \in [t_0, T] \tag{60}$$

which consists of an ordinary differential equation (ODE), $(60)_1$ and initial conditions, $(60)_2$.

In $(60)_1$ we discard for notational convenience the argument $\boldsymbol{C}$, but keep in mind, that in computational inelasticity

Table 15 Solution of an ODE using IRK methods

(I)	Solve the set of nonlinear equations for the *stage solutions* $\boldsymbol{Z}_{ni}$ $\boldsymbol{Z}_{ni} = z_n + \Delta t \sum_{j=1}^{s} a_{ij} \boldsymbol{f}(t_{nj}, \boldsymbol{Z}_{nj}) \quad i = 1, \ldots, s.$ (66)
(II)	Compute the *stage derivatives* $\dot{\boldsymbol{Z}}_{ni}$ $\dot{\boldsymbol{Z}}_{ni} = \boldsymbol{f}(t_{ni}, \boldsymbol{Z}_{ni}) \quad i = 1, \ldots, s.$ (67)
(III)	Calculate the approximation of z at time t_{n+1} $z_{n+1} = z_n + \Delta t \sum_{i=1}^{s} b_i \dot{\boldsymbol{Z}}_{ni}.$ (68)

the IVP is coupled to the space-discrete, variational form of a BVP that is solved by finite elements resulting in displacements $\boldsymbol{u}$ and total strains $\boldsymbol{C}$, cf. Fig. 1.

The total time interval is decomposed into subintervals $t_0 < t_1 < \ldots < t_n < \ldots < t_{n+1} < \ldots < t_N = T$, the *time steps* with time step size $\Delta t_n = t_{n+1} - t_n$, $0 \le n \le N$. Assuming that the exact solution at t_n is given as $z(t_n)$, the solution at t_{n+1} is searched

$$z(t_{n+1}) = z(t_n) + \int_{t_n}^{t_{n+1}} \boldsymbol{f}(t, z(t))\, \mathrm{d}\tau. \tag{61}$$

For the numerical solution $z_{n+1} \approx z(t_{n+1})$ the integral is calculated by a single-step quadrature rule consisting of s stages

$$z_{n+1} = z(t_n) + \Delta t_n \sum_{i=1}^{s} b_i \boldsymbol{f}\left(t_n + c_i \Delta t_n, z(t_n + c_i \Delta t_n)\right) \tag{62}$$

with the weighting factors $b_i, i = 1, \ldots, s$ and the coefficients $c_i, i = 1, \ldots, s$ where the latter define (new) time *stages* $t_{ni} = t_n + c_i \Delta t_n$. The unknowns $z(t_n + c_i \Delta t_n)$ are calculated by a second integration step in analogy to (62) employing the same stages c_i but along with the weighting factors a_{ij} building the *Runge-Kutta-Matrix* $A = (a_{ij})_{i,j=1,\ldots,s}$, hence

$$z(t_n + c_i \Delta t_n) \approx \boldsymbol{Z}_{ni} \quad = z(t_n) + \Delta t_n \sum_{j=1}^{s} a_{ij} \boldsymbol{f}(t_{nj}, \boldsymbol{Z}_{nj}), \quad i = 1, \ldots, s. \tag{63}$$

With the *stage derivatives* $\dot{\boldsymbol{Z}}_{nj} := \boldsymbol{f}(t_{nj}, \boldsymbol{Z}_{nj})$ we can rewrite (63) as

$$\boldsymbol{Z}_{ni} = z(t_n) + \Delta t_n \sum_{j=1}^{s} a_{ij} \dot{\boldsymbol{Z}}_{nj}, \qquad i = 1, \ldots, s. \tag{64}$$

Hence, $\boldsymbol{Z}_{ni}$ and $\dot{\boldsymbol{Z}}_{ni}$ are two sets of unknowns which are related by (64). With the stage derivatives $\dot{\boldsymbol{Z}}_{ni}$ the update for z_{n+1} is obtained from

Table 16 Butcher arrays for (*left*) implicit RK (IRK) methods, (*center*) for diagonally implicit RK (*DIRK*) methods, (*right*) for stiffly accurate DIRK methods

$$\begin{array}{c|ccc} c_1 & a_{11} & \ldots & a_{1s} \\ \vdots & \vdots & \ddots & \vdots \\ c_s & a_{s1} & \ldots & a_{ss} \\ \hline & b_1 & \ldots & b_s \end{array} \qquad \begin{array}{c|ccc} c_1 & a_{11} & \ldots & 0 \\ \vdots & \vdots & \ddots & \vdots \\ c_s & a_{s1} & \ldots & a_{ss} \\ \hline & b_1 & \ldots & b_s \end{array} \qquad \begin{array}{c|ccc} c_1 & a_{11} & \ldots & 0 \\ \vdots & \vdots & \ddots & \vdots \\ 1 & b_1 & \ldots & b_s \\ \hline & b_1 & \ldots & b_s \end{array}$$

$$z_{n+1} = z_n + \Delta t_n \sum_{i=1}^{s} b_i \dot{\boldsymbol{Z}}_{ni}. \tag{65}$$

In summary, the solution of the IVP of the format (60) by a fully implicit RK method is obtained by the algorithm of Table 15.

A typical representation of RK methods is the *Butcher-array*, see Table 16. Fully implicit RK methods exhibit an upper triangle (i.e. $j > i$) matrix with at least one entry $a_{ij} \neq 0$, $j > i$. This means that all stage values $\boldsymbol{Z}_{ni}$ are coupled. For explicit RK methods it holds $a_{ij} = 0$, for $j \ge i$.

If the coefficients fulfil the two conditions

$$\begin{array}{ll} (i) & b_i \ge 0, \qquad\qquad\qquad\qquad\qquad\qquad i = 1, \ldots, s \\ (ii) & M := (b_i a_{ij} + b_j a_{ji} - b_i b_j)_{i,j=1,\ldots,s} \text{ is positive semidefinite,} \end{array}$$

the scheme is called *algebraic stable*. It can be shown that algebraic stable, implicit RK-methods are B-stable (and for that reason A-stable as well), [19].

Stiffly accurate DIRK schemes

For the particular strength (and the very definition) of DIRK methods, we cite Alexander in [1]: *'To integrate a system of n differential equations, an implicit method with full $s \times s$ matrix requires the solution of ns simultaneous implicit (in general nonlinear) equations in each time step (...). One way to circumvent this difficulty is to use a lower triangular matrix (a_{ij}) (i.e. a matrix with $a_{ij} = 0$ for $i < j$); the equations may then be solved in s successive stages with only an n-dimensional systems to be solved at each stage.'*

The lower triangle structure of the matrix $A = (a_{ij})$, $i, j = 1, \ldots, s$ enables an algorithmic procedure of the multi-stage

method which is analogous to the single-stage BE; the procedure is a marching forward through the time interval, from stage to stage, where the subproblem in each stage is like BE.

Since DIRK methods are strongly S-stable, they can be applied for inelastic problems, which are typically stiff. The concept of S-stability was introduced in [37] in view of the fact, that A-stability turned out to be not sufficient for stiff problems.

An s-stage DIRK method exhibits consistency order $p = s$ for $p = 1, 2, 3$, for order 4 however, at least 5 stages are necessary. For a comprehensive description of DIRK methods we refer to [19] and for original papers dealing with (embedded) DIRK methods to [5,1]. For the application of DIRK methods within the DAE/MLNA approach we refer to [11,12,22].

For a *stiffly accurate* RK-scheme, step (II) in Table 15 can be skipped (i.e. the stage derivatives $\dot{\boldsymbol{Z}}_{ni}$ need not be calculated) since these schemes meet the requirement $a_{si} = b_i$ for all $i = 1, \ldots, s$ and the approximate solution z_{n+1} of step (III) in Table 15 coincides with the last stage solution $\boldsymbol{Z}_{ns}$

$$z_{n+1} = z_n + \Delta t_n \sum_{j+1}^{s} b_j \dot{\boldsymbol{Z}}_{nj}. \tag{69}$$

Of considerable relevance are DIRK methods, which are stiffly accurate

$$\boldsymbol{Z}_{ni} = z_n + \Delta t_n \sum_{j=1}^{i} a_{ij} \dot{\boldsymbol{Z}}_{nj} = \boldsymbol{\Sigma}_{ni} + \Delta t_n a_{ii} \dot{\boldsymbol{Z}}_{ni}\,, \tag{70}$$

where $\boldsymbol{\Sigma}_{ni}$ is the summed-up internal variable serving as initial value for the stage i

$$\boldsymbol{\Sigma}_{ni} = z_n + \Delta t_n \sum_{j=1}^{i-1} a_{ij} \dot{\boldsymbol{Z}}_{nj}. \tag{71}$$

The stage derivatives $\dot{\boldsymbol{Z}}_{nj}$ in the sum of (71) belong to previous stages as indicated by the upper limit of the summation $j_{\max} = i - 1$. For that reason they can be calculated from (70) solving for $\dot{\boldsymbol{Z}}_{ni}$ according to

$$\dot{\boldsymbol{Z}}_{ni} = \frac{\boldsymbol{Z}_{ni} - \boldsymbol{\Sigma}_{ni}}{\Delta t_n a_{ii}}. \tag{72}$$

Table 17 Butcher arrays for different stiffly accurate DIRK methods with s: number of stages, p: convergence order

(a) DIRK2 (Cash's method), $s = 2, p = 2$, [1], p.1012.

$$\begin{array}{c|cc} \alpha & \alpha & \\ 1 & 1-\alpha & \alpha \\ \hline & 1-\alpha & \alpha \end{array} \qquad \alpha = 1 - \frac{1}{2}\sqrt{2}$$

(b) DIRK3 (Cash's method), $s = 3, p = 3$, [1], p.1012.

$$\begin{array}{c|ccc} \gamma & \gamma & & \\ \delta & \tau-\gamma & \gamma & \\ 1 & \alpha & \beta & \gamma \\ \hline & \alpha & \beta & \gamma \end{array}$$

$$\begin{aligned} \alpha &= 1.2084966491760101 \\ \beta &= -0.6443631706844691 \\ \gamma &= 0.4358665215084580 \\ \delta &= 0.7179332607542295 \\ \tau-\gamma &= 0.2820667392457705 \end{aligned}$$

(c) DIRK4 (Cash's method), $s = 5, p = 4$, [5], p.296.

$$\begin{array}{c|ccccc} \tau_1 & \alpha & & & & \\ \tau_2 & \alpha_{21} & \alpha & & & \\ \tau_3 & \alpha_{31} & \alpha_{32} & \alpha & & \\ \tau_4 & \alpha_{41} & \alpha_{42} & \alpha_{43} & \alpha & \\ 1 & b_1 & b_2 & b_3 & b_4 & \alpha \\ \hline & b_1 & b_2 & b_3 & b_4 & \alpha \end{array}$$

$$\begin{aligned} \alpha &= 0.4358665215 \\ \alpha_{21} &= -1.13586652150 \\ \alpha_{31} &= 1.08543330679 \\ \alpha_{32} &= -0.721299828287 \\ \alpha_{41} &= 0.416349501547 \\ \alpha_{42} &= 0.190984004184 \\ \alpha_{43} &= -0.118643265417 \end{aligned} \qquad \begin{aligned} \tau_1 &= \alpha \\ \tau_2 &= -0.7 \\ \tau_3 &= 0.8 \\ \tau_4 &= 0.924556761814 \\ b_1 &= 0.896869652944 \\ b_2 &= 0.0182725272734 \\ b_3 &= -0.0845900310706 \\ b_4 &= -0.266418670647 \end{aligned}$$

(d) DIRK4 (Hairer & Wanner), $s = 5$, $p = 4$, [19], p.100.

$$\begin{array}{c|ccccc} \frac{1}{4} & \frac{1}{4} & & & & \\ \frac{3}{4} & \frac{1}{2} & \frac{1}{4} & & & \\ \frac{11}{20} & \frac{17}{50} & -\frac{1}{25} & \frac{1}{4} & & \\ \frac{1}{2} & \frac{371}{1360} & -\frac{137}{2720} & \frac{15}{544} & \frac{1}{4} & \\ 1 & \frac{25}{24} & -\frac{49}{48} & \frac{125}{16} & -\frac{85}{12} & \frac{1}{4} \\ \hline & \frac{25}{24} & -\frac{49}{48} & \frac{125}{16} & -\frac{85}{12} & \frac{1}{4} \end{array}$$

RK tableaus for DIRK schemes which are used in the present work, are displayed in Table 17.

References

1. Alexander R (1977) Diagonally implicit Runge-Kutta methods for stiff O.D.E'.s. SIAM J Numer Anal 14:1006–1021
2. Bergstrøm JS, Boyce MC (1998) Constitutive modeling of the large strain time-dependent behavior of elastomers. J Mech Phys Solids 46:931–954
3. Bergstrøm JS, Boyce MC (1998) Constitutive modeling of the time-dependent and cyclic loading of elastomers and application to soft biological tissues. Mech Mater 33:523–530
4. Büttner J (2003) Numerische Simulation zeitabhängiger Materialgleichungen mit Fließfläche (in german). PhD thesis, Fortschritts-Berichte VDI, 366
5. Cash JR (1979) Diagonally implicit Runge-Kutta formulae with error estimates. J Inst Math Appl 24:293–301
6. Dal H, Kaliske M (2009) Bergstrøm-Boyce model for nonlinear finite rubber viscoelasticity: theoretical aspects and algorithmic treatment for the FE method. Comput Mech 44:809–823
7. Ehlers W, Markert B (2001) A linear viscoelastic biphasic model for soft tissues based on the theory of porous media. J Biomech Eng Trans ASME 123(5):418–424
8. Eidel B (2011) Modeling and numerical analysis of inelasticity on and across multiple length scales. University of Duisburg-Essen, Habilitation-Thesis
9. Eidel B, Kuhn C (2011) Order reduction in computational inelasticity: why it happens and how to overcome it–the ODE case of viscoelasticity. Int J Numer Methods Eng 87(11):1046–1073

10. Eidel B, Kuhn C (2012) Is there an order barrier $p \leq 2$ for time integration in computational elasto-plasticity? Submitted for publication
11. Ellsiepen P (1999) Zeit- und ortsadaptive Verfahren angewandt auf Mehrphasenprobleme poröser Medien (in german). PhD thesis, Universität Stuttgart
12. Ellsiepen P, Hartmann P (2001) Remarks on the interpretation of current nonlinear finite element analyses as differential-algebraic equations. Int J Numer Methods Eng 51:679–707
13. Fancello E, Ponthot J-P, Stainier L (2006) A variational formulation of constitutive models and updates in non-linear finite viscoelasticity. Int J Numer Methods Eng 65:1831–1864
14. Govindjee S (2004) Numerical issues in finite elasticity and viscoelasticity. In: Saccomandi G, Ogden RW (eds) Mechanics and thermomechanics of rubberlike solids. CISM courses and lectures, vol 452, Springer, New York, pp 187–232
15. Groß M, Betsch P (2010) Energy-momentum consistent finite element discretization of dynamic finite viscoelasticity. Comput Meth Appl Mech Eng 81:1341–1386
16. Hairer E (1980) Highest possible order of algebraically stable diagonally implicit Runge-Kutta methods. Bit 20:254–256
17. Hairer E, Wanner G (2002) Solving ordinary differential equations II, stiff and differential-algebraic problems, Corr. 2nd printing. Springer, Berlin
18. Hairer E, Lubich Ch, Roch M (1989) The numerical solution of differential-algebraic systems by Runge-Kutta methods. Lecture notes in mathematics, vol 1409. Springer, Berlin.
19. Hairer E, Nørsett SP, Wanner G (2008) Solving ordinary differential equations I, nonstiff problems, 2nd revised edition, corr. 3rd printing. Springer, Berlin
20. Hartmann S (2002) Computation in finite strain viscoelasticity: finite elements based on the interpretation as differential-algebraic equations. Comput Meth Appl Mech Eng 191:1439–1470
21. Hartmann S, Wensch J (2007) Finite element analysis of viscoelastic structures using Rosenbrock-type methods. Comput Mech 40:383–398
22. Hartmann S (2003) Finite-elemente Berechnung inelastischer Kontinua–interpretation als algebro-differentialgleichungssysteme (in german). Universität Kassel, Habilitation thesis
23. Hartmann S (2005) A remark on the application of the Newton-Raphson method in non-linear finite element analysis. Comput Meth Appl Mech Eng 36:100–116
24. Hartmann S, Neff P (2003) Polyconvexity of generalized polynomial-type hyperelastic strain energy functions for near-incompressibility. Int J Solids Struct 40(11):2767–2791
25. Haupt P (2002) Continuum mechanics and theory of materials, 2nd edn. Springer, New York
26. Holzapfel GA (1996) On large strain viscoelasticity: continuum formulation and finite element applications to elastomeric structures. Int J Numer Methods Eng 39:3903–3926
27. Huber N, Tsakmakis C (2000) Finite deformation viscoelasticity laws. Mech Mater 32:1–18
28. Kröner E (1960) Allgemeine Kontinuumstheorie der Versetzungen und Eigenspannungen. Arch Ration Mech Anal 4:273–334
29. Lakes RS (1998) Viscoelastic solids. CRC Press, Boca Raton
30. Lee EH (1969) Elastic-plastic deformation at finite strains. ASME J Appl Mech 36:1–6
31. Le Tallec P (2007) Numerical methods for nonlinear viscoelastic problems in continuum mechanics. École Polytechnique, Département de Mécanique, version 1. Paris, Oct 2007
32. Lion A (1997) On the large deformation behaviour of reinforced rubber at different temperatures. J Mech Phys Solids 2045(11–12):1805–1834
33. Lion A, Kardelky C (2004) The Payne effect in finite viscoelasticity: constitutive modelling based on fractional derivatives and intrinsic time scales. Int J Plast 20(7):1313–1345
34. Markert B (2008) A biphasic continuum approach for viscoelastic high-porosity foams: comprehensive theory, numerics, and application. Arch Comput Methods Eng 15:371–446
35. Miehe C, Göktepe S (2005) A micro-macro approach to rubber-like materials. Part II: the micro-sphere model of finite rubber viscoelasticity. J Mech Phys Solids 53:2231–2258
36. Nagtegaal JC (1982) On the implementation of inelastic constitutive equations with special reference to large deformation problems. Comput Meth Appl Mech Eng 33:469–484
37. Prothero A, Robinson A (1974) On the stability and accuracy of one-step methods for solving stiff systems of ordinary differential equations. Math Comput 28:145–162
38. Reese S, Govindjee S (1998) A theory of finite viscoelasticity and numerical aspects. Int J Solids Struct 35:3455–3482
39. Simó JC (1998) Modelling and simulation of plasticity. In: Ciarlet PG, Lions JL (eds) Handbook of numerical analysis, vol 6. Numerical methods for solids (Part 3). Elsevier, Amsterdam, pp 183–499
40. Simó JC, Taylor RL (1985) Consistent tangent operators for rate-independent elastoplasticity. Comput Meth Appl Mech Eng 48:101–118
41. Vaziri A, Gopinath A (2008) Cell and biomolecular mechanics in silico. Nature 7:15–23
42. Zienkiewicz OC, Taylor RL (2000) The finite element method, 5th edn, vols 1–3. Butterworth-Heinemann, Oxford